TECHNICAL REPORT RE-83-21

A Digital Beamforming Array

J. M. Loomis
J. F. Rose
Advanced Sensors Directorate
US Army Missile Laboratory

May 1983

U.S. ARMY MISSILE COMMAND
Redstone Arsenal, Alabama 35898

Approved for public release;
distribution unlimited.

DISPOSITION INSTRUCTIONS

DESTROY THIS REPORT WHEN IT IS NO LONGER NEEDED. DO NOT RETURN IT TO THE ORIGINATOR.

DISCLAIMER

THE FINDINGS IN THIS REPORT ARE NOT TO BE CONSTRUED AS AN OFFICIAL DEPARTMENT OF THE ARMY POSITION UNLESS SO DESIGNATED BY OTHER AUTHORIZED DOCUMENTS.

TRADE NAMES

USE OF TRADE NAMES OR MANUFACTURERS IN THIS REPORT DOES NOT CONSTITUTE AN OFFICIAL INDORSEMENT OR APPROVAL OF THE USE OF SUCH COMMERCIAL HARDWARE OR SOFTWARE.

SECURITY CLASSIFICATION OF THIS PAGE (When Data Entered)

REPORT DOCUMENTATION PAGE

READ INSTRUCTIONS BEFORE COMPLETING FORM

1. REPORT NUMBER: TR-RE-83-21	2. GOVT ACCESSION NO.: AD A12 615
3. RECIPIENT'S CATALOG NUMBER:	
4. TITLE (and Subtitle): A Digital Beamforming Array	5. TYPE OF REPORT & PERIOD COVERED: Technical Report
	6. PERFORMING ORG. REPORT NUMBER:
7. AUTHOR(s): J. M. Loomis J. F. Rose	8. CONTRACT OR GRANT NUMBER(s):
9. PERFORMING ORGANIZATION NAME AND ADDRESS: Commander, US Army Missile Command ATTN: DRSMI-RER Redstone Arsenal, AL 35898	10. PROGRAM ELEMENT, PROJECT, TASK AREA & WORK UNIT NUMBERS:
11. CONTROLLING OFFICE NAME AND ADDRESS: Commander, US Army Missile Command ATTN: DRSMI- RPT Redstone Arsenal, AL 35898	12. REPORT DATE: May 1983 13. NUMBER OF PAGES: 92
14. MONITORING AGENCY NAME & ADDRESS (if different from Controlling Office):	15. SECURITY CLASS. (of this report): Unclassified 15a. DECLASSIFICATION/DOWNGRADING SCHEDULE:

16. DISTRIBUTION STATEMENT (of this Report)

Approved for public release; distribution unlimited.

17. DISTRIBUTION STATEMENT (of the abstract entered in Block 20, if different from Report)

18. SUPPLEMENTARY NOTES

19. KEY WORDS (Continue on reverse side if necessary and identify by block number)

Array
Digital Beamforming
Multi-receiver array
Array Signal Processing

20. ABSTRACT (Continue on reverse side if necessary and identify by block number)

An eight element Digital Beamforming (DBF) array is described. The array has the capability of forming multiple simultaneous beams by converting the RF amplitude and phase of each element to a digital format followed by beamforming in a general purpose computer. The subassemblies necessary at each element for down-conversion and amplification were measured in terms of phase and amplitude matching between elements. Antenna pattern data was gathered and a variety of antenna patterns are presented. Analysis is performed on the patterns to quantify the errors. These errors are compared to the effors measured on the subassemblies to verify the error effects.

DD FORM 1 JAN 73 1473 EDITION OF 1 NOV 65 IS OBSOLETE

SECURITY CLASSIFICATION OF THIS PAGE (When Data Entered)

TABLE OF CONTENTS

LIST OF TABLES

LIST OF FIGURES

I. INTRODUCTION

An eight-element, multireceiver array is presented which forms beams through the transformation of the analog elemental information to a digital format for subsequent processing in a general purpose computer. The relative amplitude and phase received by each element are maintained through use of a gain and phase matched receiver following each of the elements. The receivers amplify and down-convert the RF signals into inphase and quadrature components at a level appropriate for analog to digital conversion. From a sample of the inphase and quadrature channels from each element, a variety of beam patterns can be formed, including sum and difference patterns, patterns with reduced sidelobes, and patterns with nulls at specified locations in angular space.

The concept of forming receive antenna beams by combining the elements amplitude and phase at an intermediate frequency or in a digital computer has been pursued for many years [1, 2, 3]. This technique which has been called array signal processing or digital beamforming (DBF) has the primary advantage of being capable of forming flexible multiple beams through the use of parallel digital algorithms such as Fast Fourier Transform (FFT's) rather than replicating different microwave feeds. In addition, having a digital representation of the coherent amplitude and phase at each element gives the potential to perform adaptive beamforming, or nulling [4, 5] and extended resolution techniques such as maximum entropy [6, 7].

In the previous research into DBF, the technique has been shown

to be feasible, especially for arrays with a small number of elements. DBF has been used in active radar height finding applications, passive direction finding, and HF surveillance systems. The primary impediment to DBF being used in other radar applications is that the computational load on the beam forming processor is severe, especially for typical radar data rates of between 100 KHz and 50 MHz. Moreover, in larger arrays the element module cost must be made low enough to compete effectively with current technology.

Many new developments are occurring in electronic components and these advances now make it possible to consider DBF for large radar applications. For example, recent increases in computational speeds and the development of high speed, low cost analog to digital converters have brought processor capabilities up to levels necessary to support many radar requirements. In addition, the RF and IF components being developed for microwave monolithic circuits offer the very real possibility of reduced size, cost, and power consumption necessary to afford and package a receive/down-conversion module behind each element.

The signal conditioning and combining network shown in Figure 1 can take many forms depending on the application. The applications vary from a simple combining network that produces a fixed beam pointing only one direction in space to networks which are capable of forming multiple beams, scanned in space. In addition, different illumination functions can be formed in the combining network in order to reduce sidelobes, form nulls, or create broadened beams. This section will describe some of the techniques currently being used for

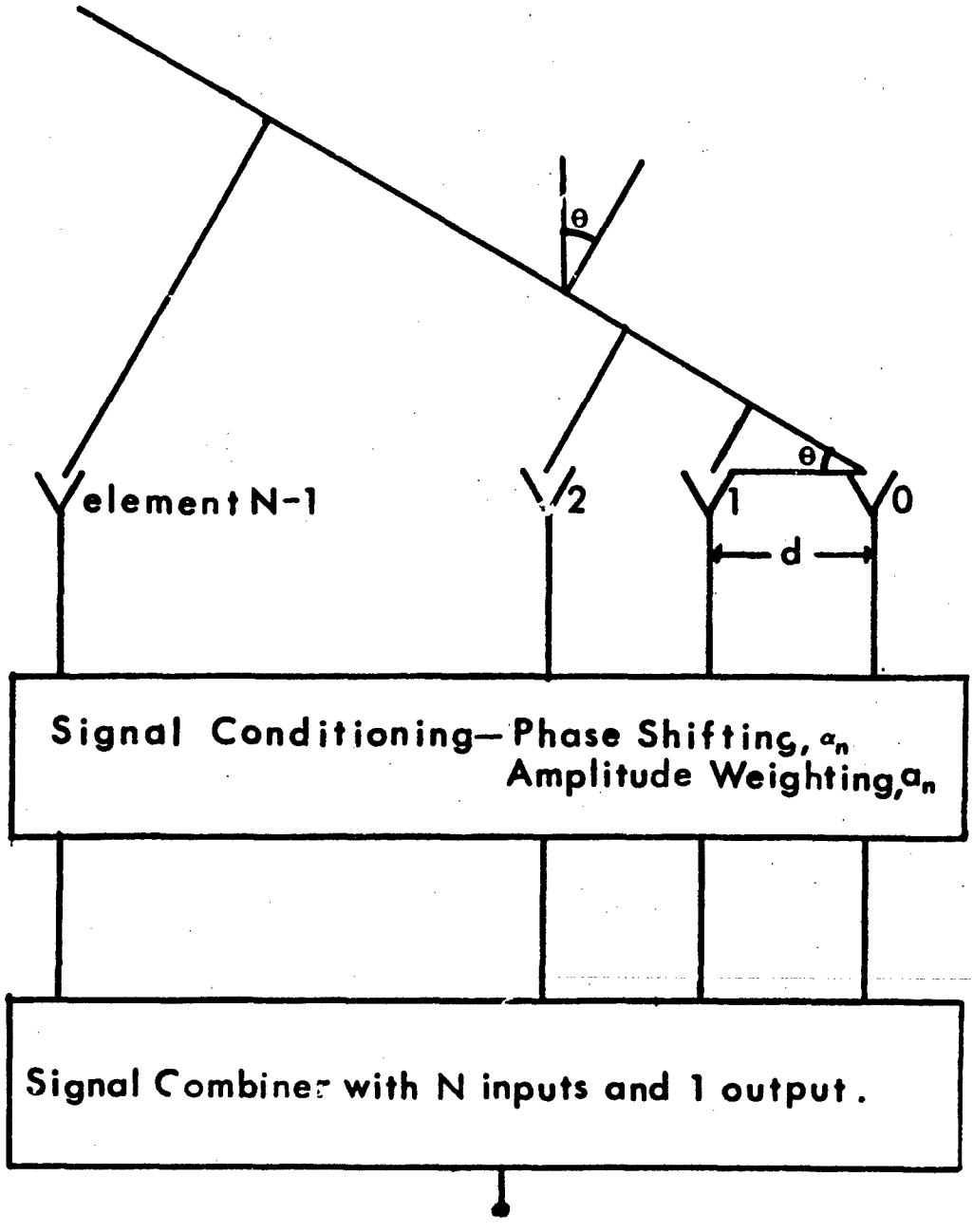

Figure 1. Block diagram of antenna array system

conditioners and combiners. Since DBF is a receive only technique, the emphasis in this discussion will be on receive combiners.

A common radar use for arrays involves electronic scanning of a single beam through the use of variable phase shifters at each element. Depending on the application, an amplitude taper may also be applied to the elements before combining to obtain a low sidelobe pattern. The weights are usually applied at the operating frequency so that they can be conveniently used for both transmit and receive. The phase shifting techniques include changing the reactance in a transmission media or changing the path length (time delay) through an element. Phase shifters can be constructed, for example, using a ferrite material in a waveguide. In a ferrite, the phase velocity of electromagnetic waves can be controlled by varying an external voltage applied to the material. P-I-N diodes are also used, in this instance as switches, to either change the path length, or to switch reactive components into a signal path to impose a change in impedence or phase.

As described earlier in order to shape the beam for lower sidelobes or to produce monopulse patterns, some form of amplitude control is necessary. This can be accomplished using attenuators, amplifiers of different gains, or a combining network which weights the inputs to produce a weighted sum. In each case the relative phase between elements must be preserved over the operational frequency band. Attenuating to achieve a nonuniform illumination is rather lossy in terms of signal to noise ratio (S/N) but is the most likely choice in an instance when a variable illumination function is needed, due to

the difficulty in matching the phase of many variable gain amplifiers over both frequency and gain variations. However, in practice, variable amplitude illumination functions are generally not used because of the complexity involved, but rather a fixed amplitude taper is applied in parallel through use of unequal power dividers such as directional couplers or Wilkenson dividers.

In some applications where high accuracy and resolution throughout a large scan volume are required, a single beam system may not be capable of satisfying all requirements. It has therefore been necessary to develop multiple parallel beam array systems in which the scan volume is divided among several beams. The most obvious means of realizing a multibeam system is through duplication of the receive network used in the single beam application. This is not very efficient, however, and more efficient designs have been implemented which attempt to reduce the quantity of hardware necessary to satisfy a design requirement.

The Butler Matrix [12] is an example of a multiple beam array which uses constant phase shifts to form nonscannable multiple beams as shown in Figure 2. The Butler Matrix is unique in that the technique applies only to arrays with $N=2^n$ elements where $n=1,2...$ This restriction, along with the appropriate interelement phasing (integer multiples of 360/N degrees between elements), creates N orthogonal beams which result in maximum pattern efficiency. With $\lambda/2$ element spacing and the phasing as just discussed, the beams are evenly spaced from $\theta = -90^o$ to $\theta = 90^o$, overlapping close to the 3dB point.

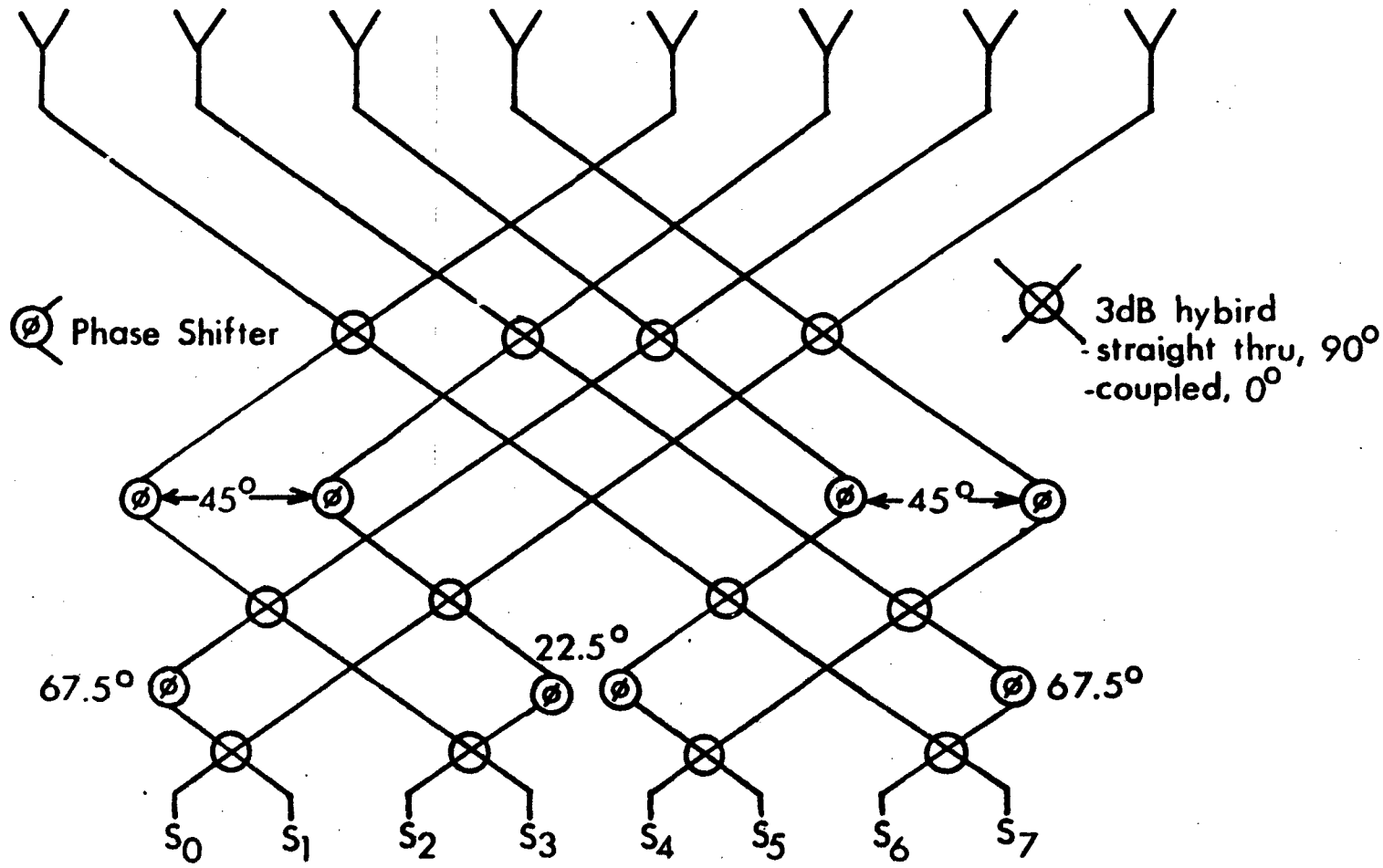

Figure 2. Eight element Butler matrix array

Other multiple beam methods use lenses as a transmission media and perform phase shifting through the distribution of the inputs and outputs on the lens. The Rotman lens [13] shown in Figure 3 is an example of this type antenna feed system. The lens is made of a dielectric located between two parallel plates to form the transmission media. There are N inputs, connected to the array elements and M outputs corresponding to the number of output beams. The location of the lens outputs and the lengths of the cables connecting the array elements to the lens are designed such that there are equal elemental phase lengths between the wavefronts arriving from the desired pointing directions and the beam output ports. The number of beams that can be implemented is dependent on the spacing necessary to obtain a good match between the lens and cable. As with the Butler Matrix, the beams of a Rotman lens are not generally scanned and there is usually a sufficient number of beams to cover the spatial volume. Amplitude tapering for both the Butler Matrix and Rotman lens can be accomplished either by attenuating the outputs or feeding more than one input with unequal weights. These techniques result in very complex feed mechanizations and are rarely used.

Another technique, called Digital Beamforming, which is the topic at hand converts the analog elemental amplitude and phase, into a digital format so that the data can be input into a digital signal processor and a combination of external and automatic control over the phase and amplitude weights can be applied. This eliminates the need for analog phase and amplitude control while being capable of easily producing multiple beams and adaptive nulls simultaneously.

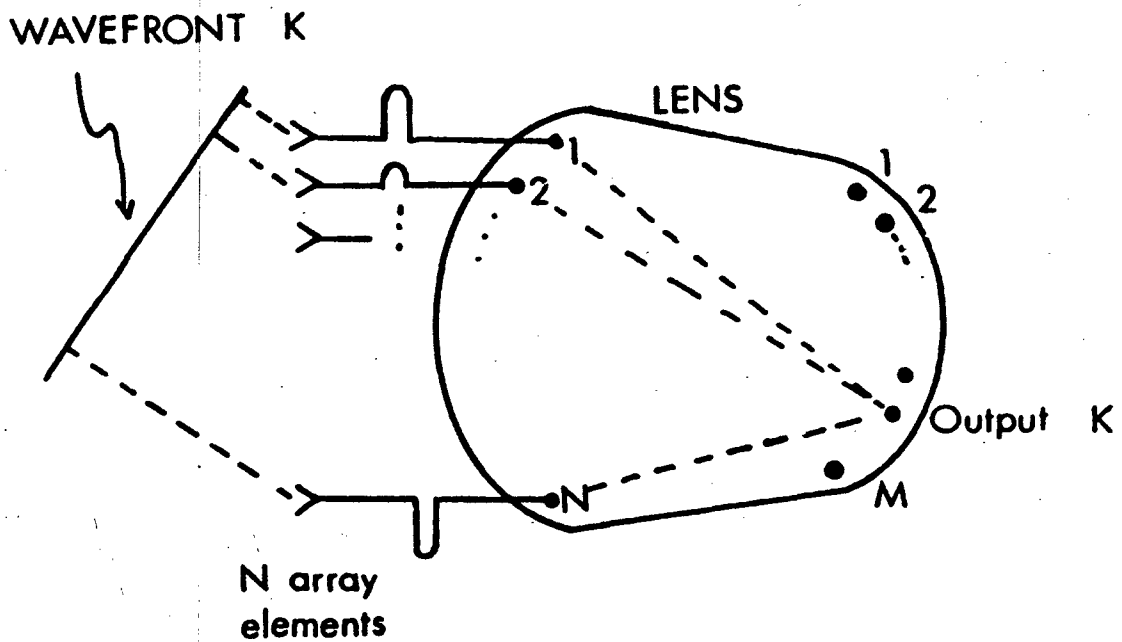

Figure 3. Rotman lens as phase shifter and combiner

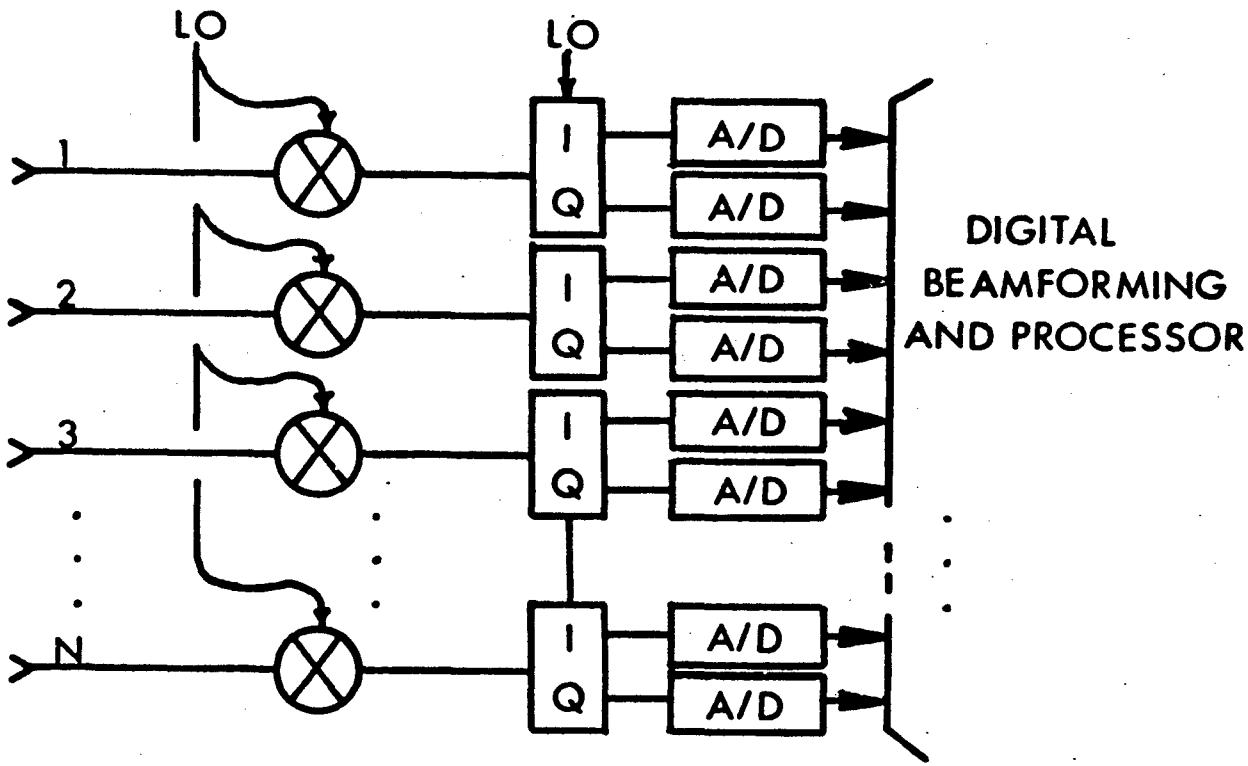

Figure 4. Digital Beamforming block diagram

Conceptually, it is possible to digitize the RF signal directly at each element with an analog-to-digital (A/D) converter; however, A/D converters which operate at RF are not yet available. Moreover, A/D converters do not have an input signal range low enough to distinguish signal levels that the elements receive ($\leq 10\mu V$); therefore both amplification and down-conversion of the RF signal are necessary before A/D conversion.

Figure 4 shows a block diagram of a network which converts the RF signal to a reduced frequency for A/D conversion. In order to steer and shape beams, the phase and amplitude of the RF signals must be preserved through the down-conversion and amplification processes.

Many similarities exist between a DBF array and a conventional array along with many subtle but important differences. In a conventional radar antenna the performance parameters are a function only of the microwave components; whereas in a DBF array not only the microwave components, but also down-conversion and digital components affect pattern performance. At the same time, radar measurement parameters such as range and radial velocity, which heretofore have been independent of the array, now are affected by the array design and element module component selection. The purpose of this effort is to design and build a prototype DBF array to quantify the effects on the antenna pattern of adding receiver circuitry and digital conversion to each array element.

The remainder of this paper consists of a development of array theory techniques under the assumption that the elements are ideal

isotropic, it leads to a development of weighting functions necessary to form and scan beams and a short discussion on some DBF peculiarities in the receiver down-conversion hardware. Section III is a description of the hardware used in this eight element array and includes the measurement of the various receive components in terms of relative phase and gain to determine the level of receiver matching obtained with this design. The antenna measurement technique is then presented and the resulting measured data is analyzed.

II. ANTENNA ARRAY THEORY

An antenna array consists of two or more radiating or receiving elements with adjacent elements usually spaced within a wavelength of one another. The exact spacing and the size, type and number of elements depends on the application for which it is to be used. The discussion herein will be based on a receive only array, in light of the topic of this paper, even though the techniques, in general, can be applied to either a transmit or receive system. The spatial response (antenna pattern) of the individual element is usually of large beamwidth, and correspondingly low gain, such that the elements essentially receive the same signal in magnitude but with possibly different phases depending on the angle of the impinging wave. A general diagram is shown in Figure 1.

The pattern (output of the signal combiner) for an equally spaced linear array with the geometry shown in Figure 1 is given by an array factor,

$$AF(\theta) = \sum_{n=0}^{N-1} a_n e^{jn(kd\sin\theta+\alpha)} \qquad (1)$$

where N is the number of elements,

d is the element spacing,

k is the wave number $2\pi/\lambda$,

λ is the operating wavelength,

a_n is the amplitude at each element,

θ is the angle of the incoming wave with respect to array normal, and

α is the incremental phase difference between elements applied in the signal conditioner.

Letting $\psi = kd\sin\theta+\alpha$, (1) becomes

$$AF(\psi) = \sum_{n=0}^{N-1} a_n e^{jn\psi} \quad . \qquad (2)$$

The terms in (2) represent the complex signal received by each element which may have been conditioned in terms of an aperture illumination function, a_n or external phasing, α_n . The array factor is used to describe some of the properties of the array given the parameters above. The properties described include the location of lobes, both major and minor, nulls and to a degree their relative amplitudes.

Letting $a_n = 1$ (uniformly illuminated) and $p = e^{j\psi}$, (2) becomes

$$AF(\psi) = \sum_{n=0}^{N-1} p^n = 1+p+p^2+\ldots p^{N-1} \qquad (3)$$

which is a polynomial with N-1 roots. The roots of the polynomial are the nulls of the array factor or through an axis transformation from ψ to θ, they are the nulls of the antenna pattern. Rewriting (3) in a product of roots form, the array factor becomes

$$AF(\psi) = \prod_{n=1}^{N-1} (p-p_n) = (1-p^N)/(1-p) \qquad (4)$$

where p_n is the n^{th} root of (3).

For example, consider an eight element uniform array, the array factor is

$$AF(\psi) = \sum_{n=0}^{7} p^n$$

$$= 1+p+p^2+\ldots+p^7$$

$$= (1-p^8)/(1-p).$$

The roots can then be calculated to be

$$\psi_n = n360°/8 \qquad (5)$$
$$= n45°, \quad n=1,2,\ldots 7.$$

The resulting antenna pattern is shown in Figure 5.

Following a procedure developed by Schelkunoff [8], the roots can be arranged around a unit circle at the angles specified by ψ_n. The array factor can be graphically determined for any angle ψ by plotting the point on the unit circle as shown in Figure 5 and calculating the product of the distance from p to each of the zeros p_n. The distances correspond to the terms of (4). In order to represent the array factor in actual angular space it is necessary to use the transformation

$$\psi = kd\sin\theta+\alpha. \qquad (6)$$

(a)

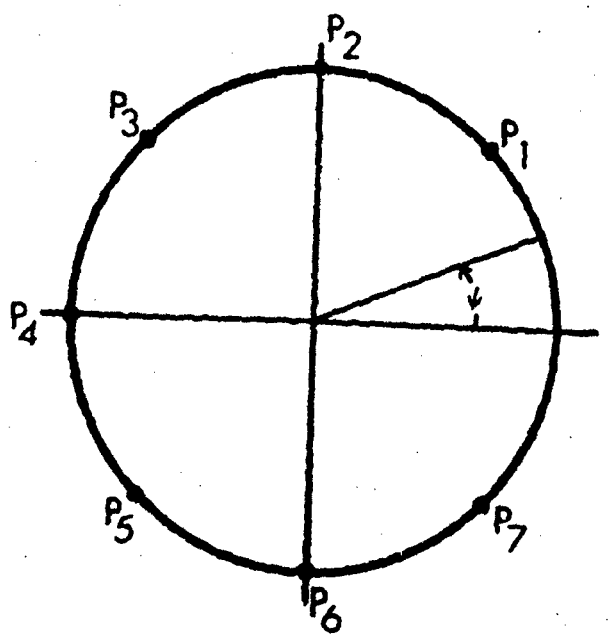

(b)

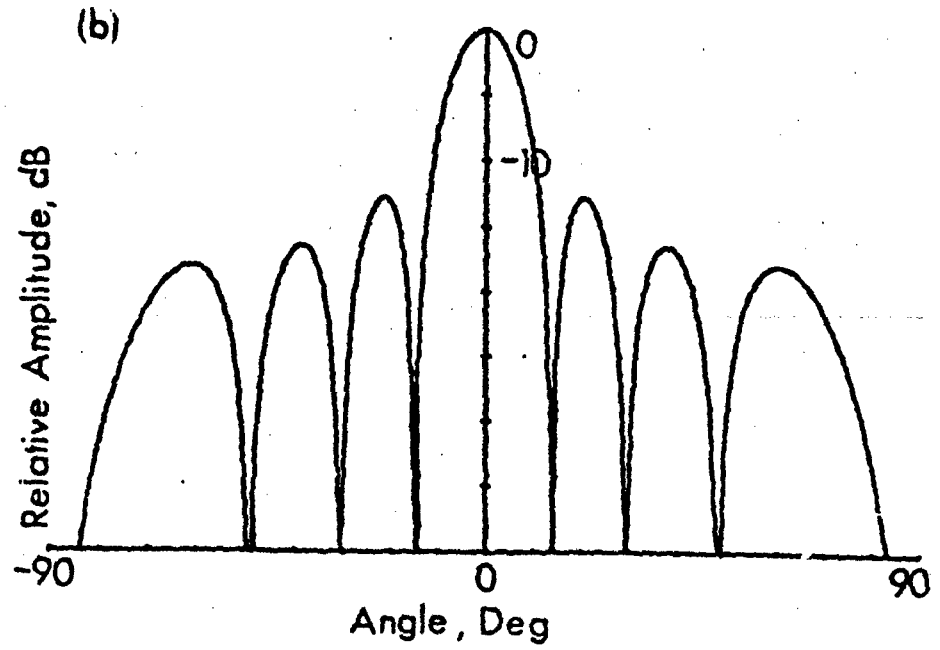

Figure 5. Location of roots (a) and resulting pattern (b) for eight element array with $\lambda/2$ spacing

It has been assumed up to this point that the array factor (1) is the radiation pattern of the antenna array system. This would hold true for isotropic radiators or elements whose response does not vary in the pattern plane. However, most real elements have a pattern which is a maximum at $\theta = 0$ and tapers off as θ increases and this is called the element pattern. The total antenna radiation pattern can then be written as the product of the array factor and the element pattern so that the antenna pattern $A(\theta)$, is written as

$$A(\theta) = AF(\theta)E(\theta)$$

where $E(\theta)$ denotes the element response in the θ plane.

Thus far, the discussion has been limited to equally spaced arrays with uniform excitation and variable interelement phase. In this way a given beam was scanned in space to point in different directions, although the relative location and magnitude of the sidelobes and nulls remained constant. Another flexibility offered by arrays is the ability to alter the excitation function to reduce the sidelobe levels and alter null locations in order to isolate the mainlobe signals from sidelobe interference. In a uniformly illuminated array the peak sidelobe levels are 12.7, 16.5 and 17.9 dB down from the mainbeam as shown in Figure 5. For interference signals more than 20 dB above the desired mainbeam signal, it is possible that the interference may become dominant and mask the desired signal. For this reason it is necessary to reduce the overall sidelobes or to position a null at the angle corresponding to the interference. Since the magnitude of the lobes is related to the spacing between adjacent roots, it follows that reducing this spacing should reduce the level

of the corresponding lobe. However, when the spacing between roots is decreased, the spacing for the mainlobe will increase resulting in a wider beamwidth.

The movement of the roots corresponds to an amplitude taper across the array. In the uniform illumination case when the roots are evenly spaced on the unit circle, the product of the terms in equation (4) result in coefficients of 1 as seen in equation (3). For the nonuniform illumination case with the roots repositioned, the coefficients resulting from the multiplication in (4) yields,

$$AF(\theta) = \prod_{n=1}^{N-1} (p-p_n)$$

$$= a_0+a_1p+a_2p^2+a_3p^3+\ldots$$

$$= \sum_{n=0}^{N-1} a_n p^n \qquad (7)$$

and these coefficients, a_n, are the relative amplitudes of each element. The coefficients necessary to produce specified sidelobe levels for arrays of various sizes can be found in [9].

As an example, to form a pattern with 30dB Chebyshev peak sidelobes for an 8 element array, the coefficients can be found from [9] and (7) can be written,

$$AF(\theta) = 0.26+0.52p+0.81p^2+1.0p^3+1.0p^4+0.81p^5+0.52p^6+.26p^7.$$

The resulting pattern is shown in Figure 6.

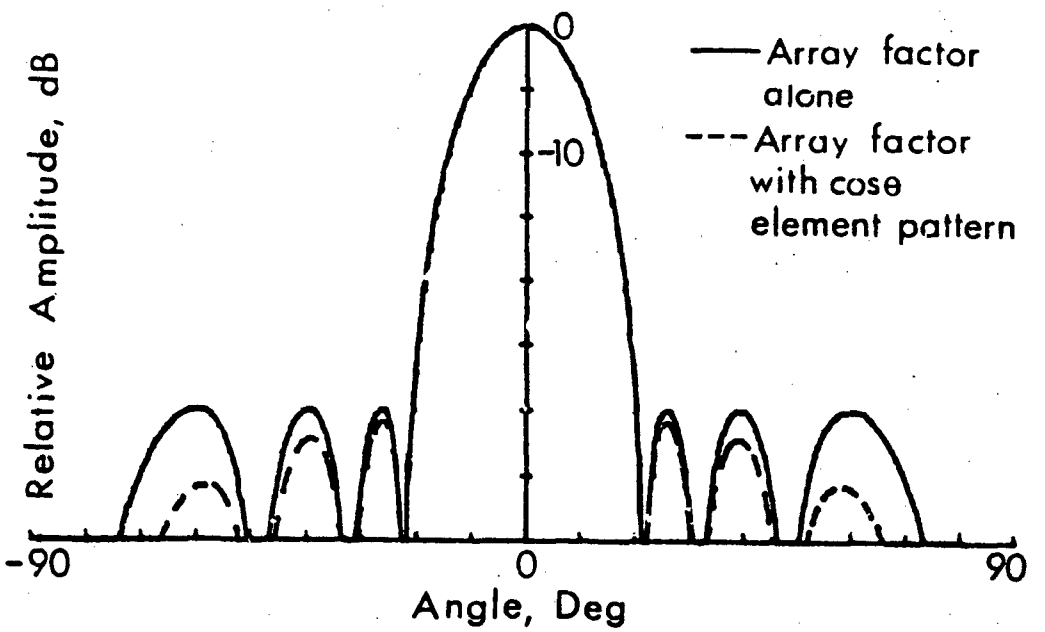

Figure 6. Antenna pattern with a 30 dB Chebyshev illumination function.

Nonuniform illumination functions can also be used to form difference patterns. A difference pattern is characterized by a null in the pointing direction and a major lobe on either side of this null. The difference pattern is used in conjunction with a single beam, or sum beam as it is better known, to accurately determine a target's angular location. The antenna is scanned in an attempt to minimize the ratio of the difference beam power to the sum beam power. The large slope of the difference pattern near the pointing direction sensitizes the receiver, which makes small changes in target angle appear as large changes in signal strength.

Referring back to the unit circle, a difference pattern can be constructed by first locating at root at $\psi = \theta = 0$. In order to

obtain major lobes on either side of this root, the remaining 6 roots (in the 8 element case) must be arranged such that the largest spacings occur between the root at $\psi = 0$ and each of its adjacent roots. Locating the roots to obtain equal spacing betwen roots p_1 through p_6 the resulting difference pattern is given in Figure 7.

The variety of antenna patterns just presented can be implemented individually in many different antenna systems. The fact that the signal combining generally takes place at the received signal frequency makes it difficult or impossible to realize all the patterns in a single system. A DBF system in which the elemental signals are down-converted to a frequency appropriate for analog to digital conversion while preserving the relative phase and amplitude between elements makes this possible. Signal preservation in the down-conversion process requires a) that the mixing process does not change the relative phase or amplitude between elements, and b) that the insertion phase and loss of the down-conversion hardware is equal, element to element.

Consider an RF signal received by an array element given by

$$E_1 = A\cos(\omega t+\phi).$$

The signal is processed by an RF mixer having a loss factor, K (which is a function of the LO power), and insertion phase, γ. The mixer has an LO signal given by

$$E_2 = B\cos[(\omega-\omega_1)t+\delta]$$

where $\omega-\omega_1$ is the frequency of the LO expressed as a difference for later convenience, and δ is the LO phase.

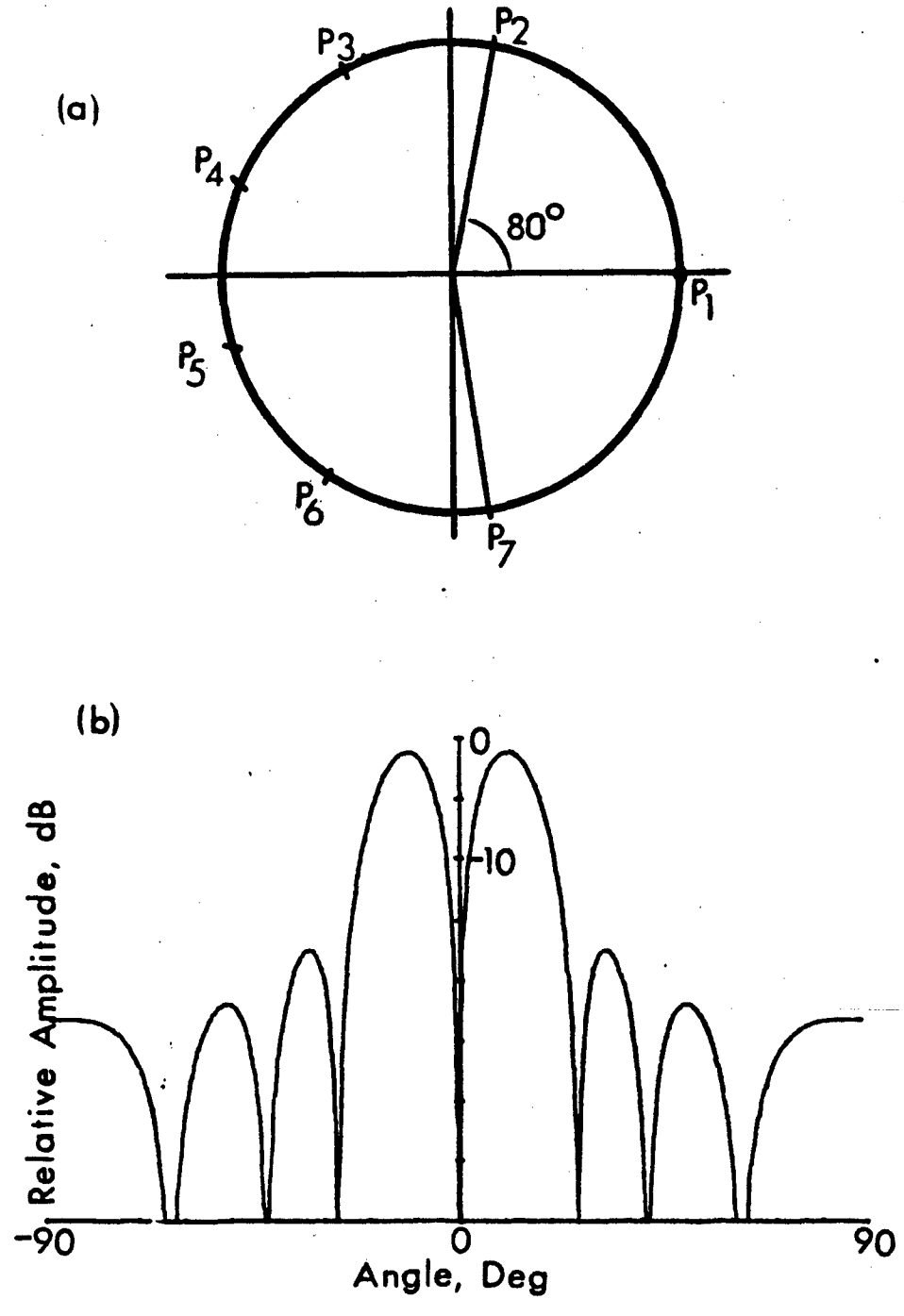

Figure 7. Location of roots (a) and resulting difference pattern (b)

The mixing process is ideally a multiplication of the input signal, E_1, and the LO, E_2, modified by the parameters K and γ. The mixer output, E_3 can be written as

$$E_3 = E_1 E_2 K \angle\gamma$$

$$= ABK \angle\gamma \{\cos(\omega t+\phi)\cos[(\omega-\omega_1)t+\delta]\}.$$

Using a trigonometric identity, E_3 can be written as the sum of two signals, one having the sum of the frequencies of E_1, and E_2, and one have the difference of the frequencies. Filtering out the sum frequency signal, E_3 can then be written as

$$E_3 = \frac{ABK}{2} \cos(\omega_1 t+\phi+\delta+\gamma).$$

Recall that the quantities to be perserved are A and ϕ, and that a similar process is performed in each element, therefore, the mixers in each element must have the same K and γ parameters. In addition, the phases and amplitudes of the LOs feeding each mixer must be the same. These restrictions dictate the need for equal path lengths in each receiver and a phase and amplitude matched LO distribution network. In actuality the loss factor (conversion loss), K, is a nonlinear function of LO signal level as shown in Figure 8 so that with a sufficient LO drive level (>4dBm) the conversion loss becomes somewhat insensitive to variations in LO signal level. Therefore, the amplitude matching of the LO network is not as critical (with efficient LO signal levels) as the phase matching, where phase differences in LOs transfer directly to the mixer outputs.

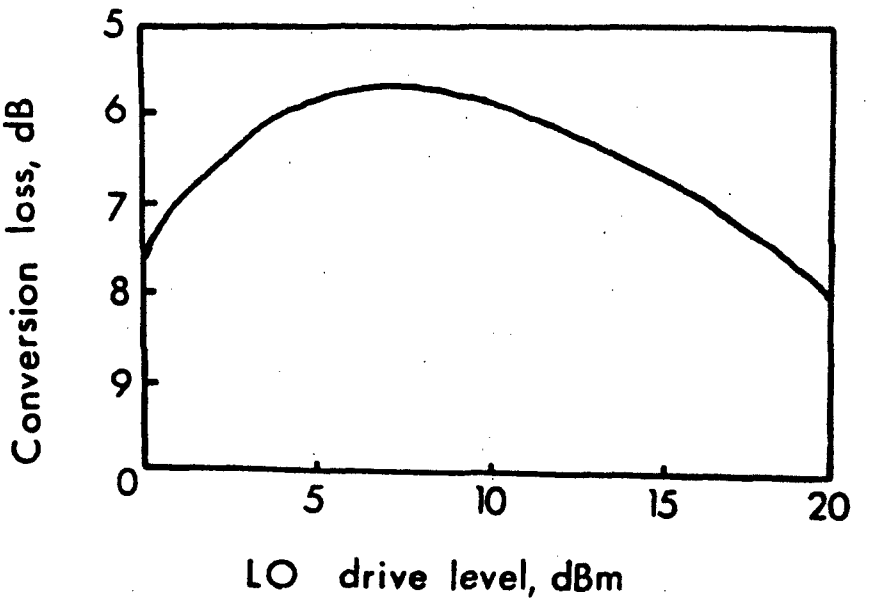

Figure 8. Conversion loss vs. LO drive level

Once the RF signals have been down-converted to an IF frequency, the phase matching becomes much easier. The wavelengths at RF are near 1" and cable connections and solder joints can effect the phase by several degrees. At IF frequencies less than 500 MHz, the wavelength is about two feet long and the receiver through phase becomes less dependent on the mechanical connections and more dependent on the transfer function characteristics of the devices. Therefore, by mixing the RF signals immediately to IF, following the array element, and amplifying and filtering etc, at the reduced frequency, the phase matching problems become less severe. Obtaining components with equal

phase and amplitude response is relatively easy at the IF frequencies and obtaining equal phase length cables to interconnect the components through to the A/D converter is also much easier.

Synchronous detection is performed during one of the down-conversion processes in order to represent the signal in a form so that the phase of the signal can be determined after digital conversion. This involves splitting the signal in each element and mixing; one with $\cos\omega t$ and the other with $\sin\omega t$ so as to produce two signals 90^{o} apart called the inphase (I) and quadrature (Q) components. This is similar to a conversion from polar coordinates to rectangular coordinates with real, I, and imaginary, Q, parts. After digitizing the I and Q signals, the phase and magnitude can be calculated from

$$A = \sqrt{I^2+Q^2}$$
$$\psi = \tan^{-1}(Q/I). \tag{8}$$

The response of the array can then be calculated in the digital processor by weighting and summing the signals from each element. The response, Y, of a particular antenna pattern designated by element weights, to a set of received and digitized data is given by

$$Y = \sum_{n=0}^{N-1} (a_n e^{j\alpha_n})(I_{n+1}+jQ_{n+1}) \tag{9}$$

$$Y = \sum_{n=0}^{N-1} (a_n e^{j\alpha_n})(A_{n+1} e^{j\psi_{n+1}})$$

where a_n and α_n are the amplitude and phase of the weighting functions, and A_n and ψ_n are the amplitude and phase of the received signal from the element.

At this point the advantage of digital beamforming becomes apparent. From a single set of digitized data, the response of numerous weighted antenna patterns can be derived from the same set of data which in effect corresponds to multiple beams with added flexibility.

The following section describes the hardware used to demonstrate this capability. The errors due to down-conversion are measured and their effects on the antenna pattern are quantified.

III. DESCRIPTION OF DBF PROTOTYPE HARDWARE

In order to gain an understanding of the Digital Beamforming technique, an eight element, X-band (9.5-10.5 GHz), linear array was designed and built. The purposes for building this prototype were to verify the concept feasibility, determine the pattern effects due to component errors, and to demonstrate the beam flexibility afforded with this approach. This chapter presents a detailed description of the components and subassemblies which were used to build the prototype array.

A block diagram of the antenna system is shown in Figure 9. Behind each receiving element of the array is a receiver to down-convert the received signal into a format suitable for digitizing. The received X-band signal is first down-converted to an IF frequency of 30 MHz, following this step both amplification and synchronous detection are performed in preparation for digital conversion of the element amplitude and phase information. Each pair of I and Q signals are cabled to one of eight baseband boards where the signals are further amplified and then digitized by an 8 bit analog-to-digital (A/D) converter. The A/D converter data is latched and output serially in 8 words, each containing 16 parallel bits (8 bits each of I and Q), into a digital processor. In addition to the in-line elemental components, two local oscillator (LO) feed networks, one variable between 9.5 and 10.5 GHz, and the other at 30 MHz, are necessary to distribute LO signals to each array element.

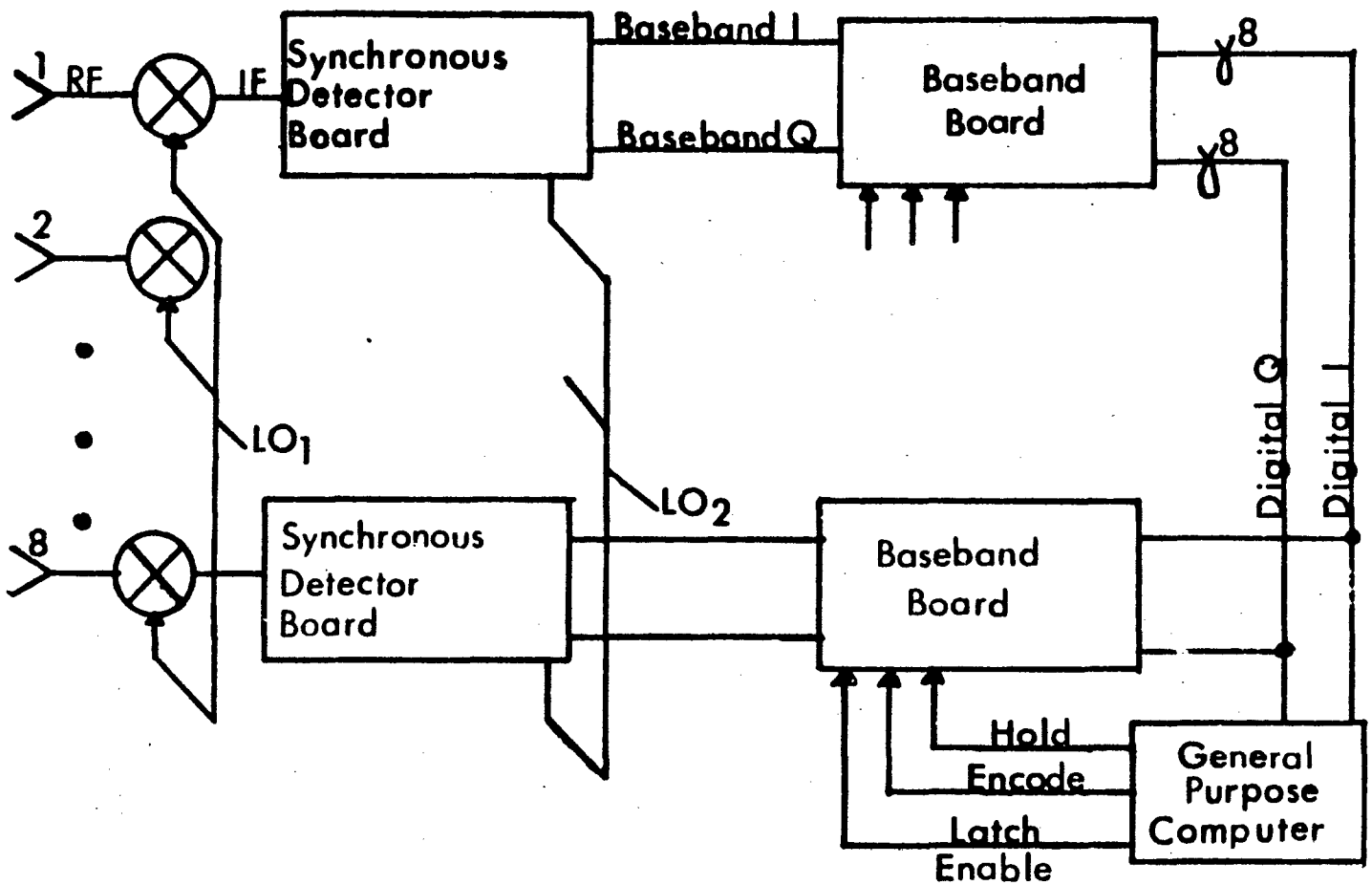

Figure 9. NBF prototype block diagram

The receiving element of the array is an H-plane sectorial horn. This horn was selected because of its simplicity and the desire to obtain some directivity in the azimuth plane while maintaining a wide element pattern in the elevation scan plane. A photograph of the antenna array is shown in Figure 10. The inter-element spacing was chosen to be 0.6" to have near $\lambda/2$ spacing and to accommodate a commercially available power divider that allowed the antenna, RF mixers and LO drive from the power divider to be connected directly. This packaging scheme eliminated the RF interconnecting cables which were felt to be a potential source of error.

The grating lobes at midband associated with 0.6" element spacing, appear at $\theta = -90^0$ when the mainlobe is scanned to 76^0. The element aperture in the elevation plane is .5375" which results in an element beamwidth of

$$BW = 50.8\ \lambda/d$$
$$= 50.8 * 1.18"/.5375"$$
$$= 112^0$$

in free space. The actual beamwidth of the element in the array environment is slightly different due to coupling effects, and will be discussed later. The azimuth beamwidth for a sectorial horn with a H-plane dimension of 6.0" is given by

$$BW_{AZ} = 68\ \lambda/d$$
$$= 13.4^0$$

Stacking the elements vertically made it mechanically difficult to use a conventional top wall coaxial to waveguide adapter or launcher; therefore, it was necessary to design an end-on launcher for this

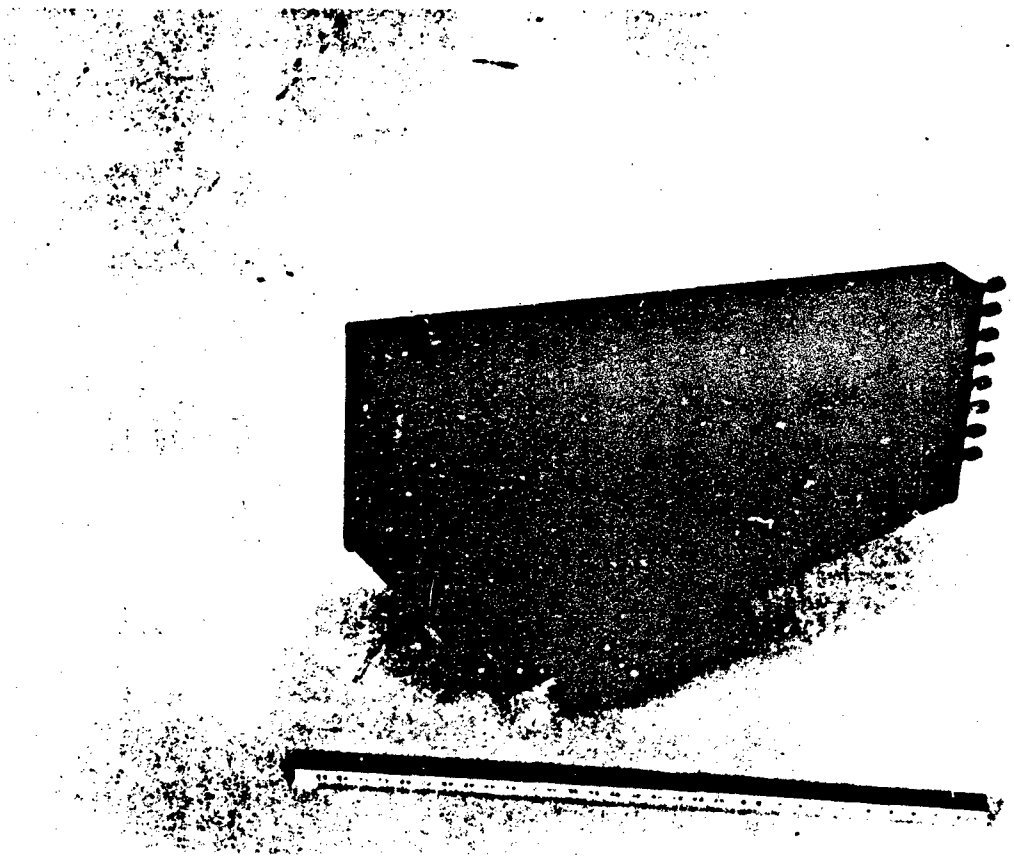

Figure 10. Horn array

application. Several launcher types including wire loops, brass strips, and brass posts were tried but in each case, either the match to free space was not adequate or the launcher was too difficult to accurately reproduce for all eight elements. A more reproducible approach was finally found based on an adaptation of a top wall design described in [14]. Figure 11 depicts the top wall adapter was well as the modified end-on version. A cut and try design process was adopted

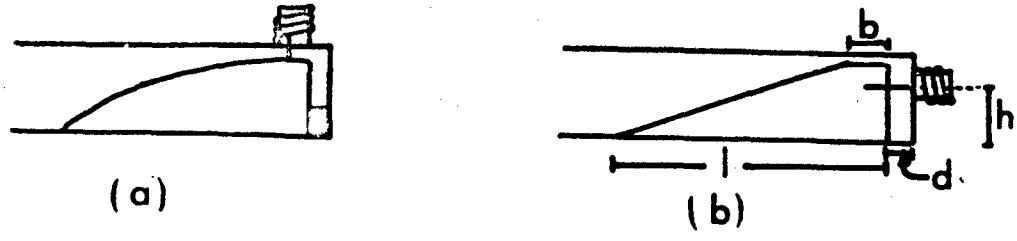

Figure 11. Conventional launcher (a) and end-on adaptation (b)

whereby the dimension, d, was varied for several lengths, l, and heights, h, to obtain a minimum reflection coefficient over the operating band. The best results were obtained with l = 2.0", b = .50", d = .10", and h = .362".

In order to establish the pattern characteristics of the array, it is necessary to account for not only reflection coefficients but also coupling effects between elements. Following a procedure described in [15], the reflection coefficient was measured for each element in the array environment. The coupling between elements was determined by exciting one element and measuring the received signal at each of the other elements with all other elements terminated properly. The

measurement procedure was performed in transmit mode with a normalized signal of 1 at 0^o applied to each element. Since a passive array is a reciprocal device, analysis can be performed in either a transmit or receive mode and the analysis will hold true for the other mode. Typical data over the frequency band is shown in Figures 12 through 15.

The antenna pattern can now be calculated for a particular frequency taking into account the mutual coupling effects and mismatch errors. The total active reflection coefficient, R_n, due to self reflection and mutual coupling at the n^{th} element can be written as [15]

$$R_n = \Gamma_n + \sum_{\substack{m=0 \\ m \neq n}}^{7} C_{mn} \quad , \tag{10}$$

where Γ_n is the complex self reflection coefficient and C_{mn} is the complex coupling from the m^{th} to the n^{th} element. Since a passive antenna is a reciprocal device the coupling measurements can be reduced by noting that $C_{mn} = C_{nm}$.

The transmission coefficient, A_n, can then be written as the sum of the applied signal and the active reflection coefficient

$$A_n = S_n + R_n \quad . \tag{11}$$

For excitations other than 1 at 0^o, the array factor is calculated by introducing a complex excitation, S_n, and combining (10) and (11)

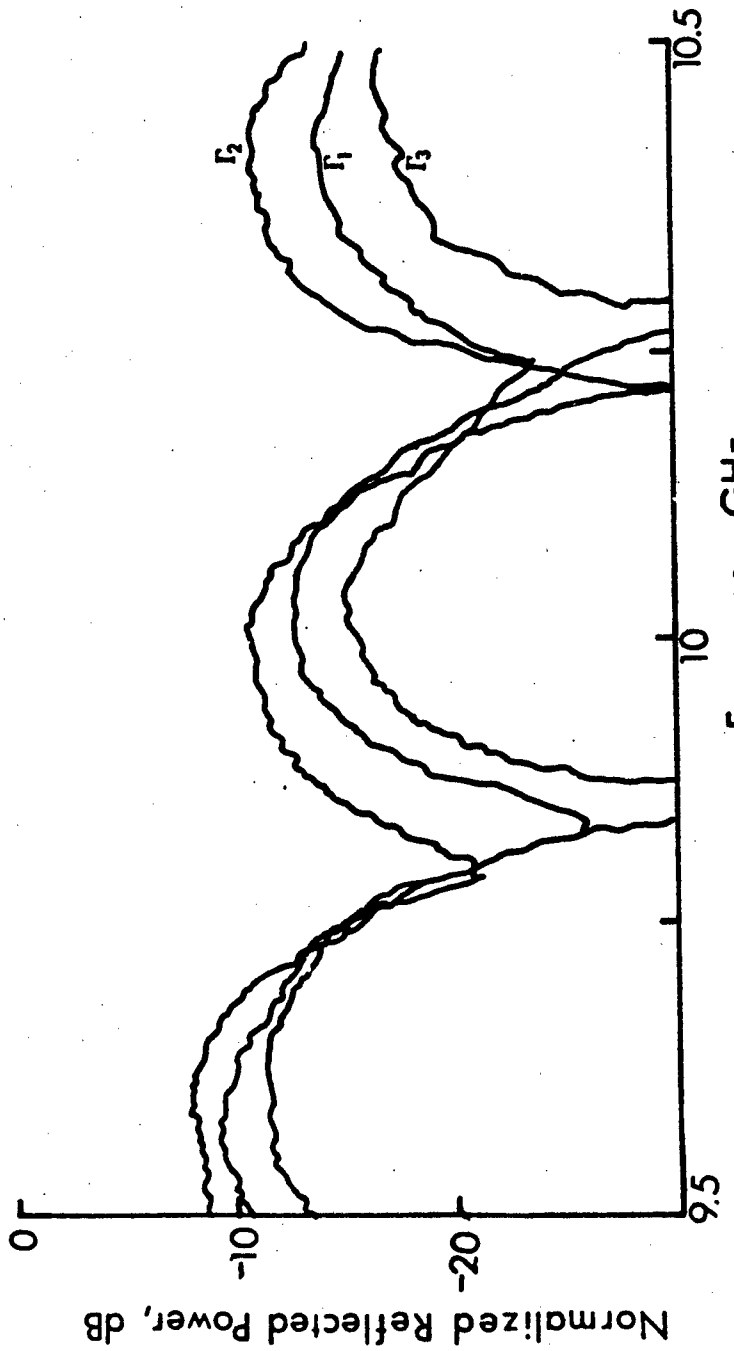

Figure 12. Typical magnitudes of reflection coefficients

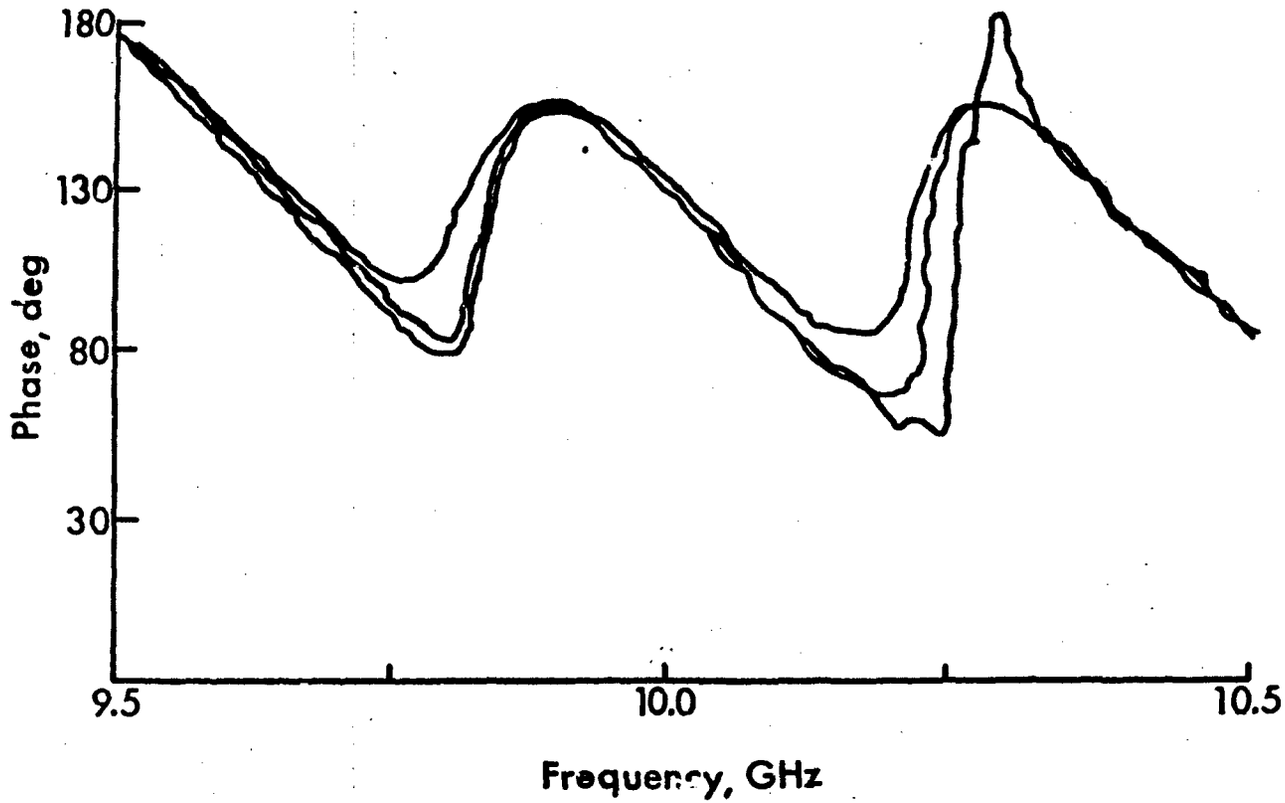

Figure 13. Typical phases of reflection coefficients

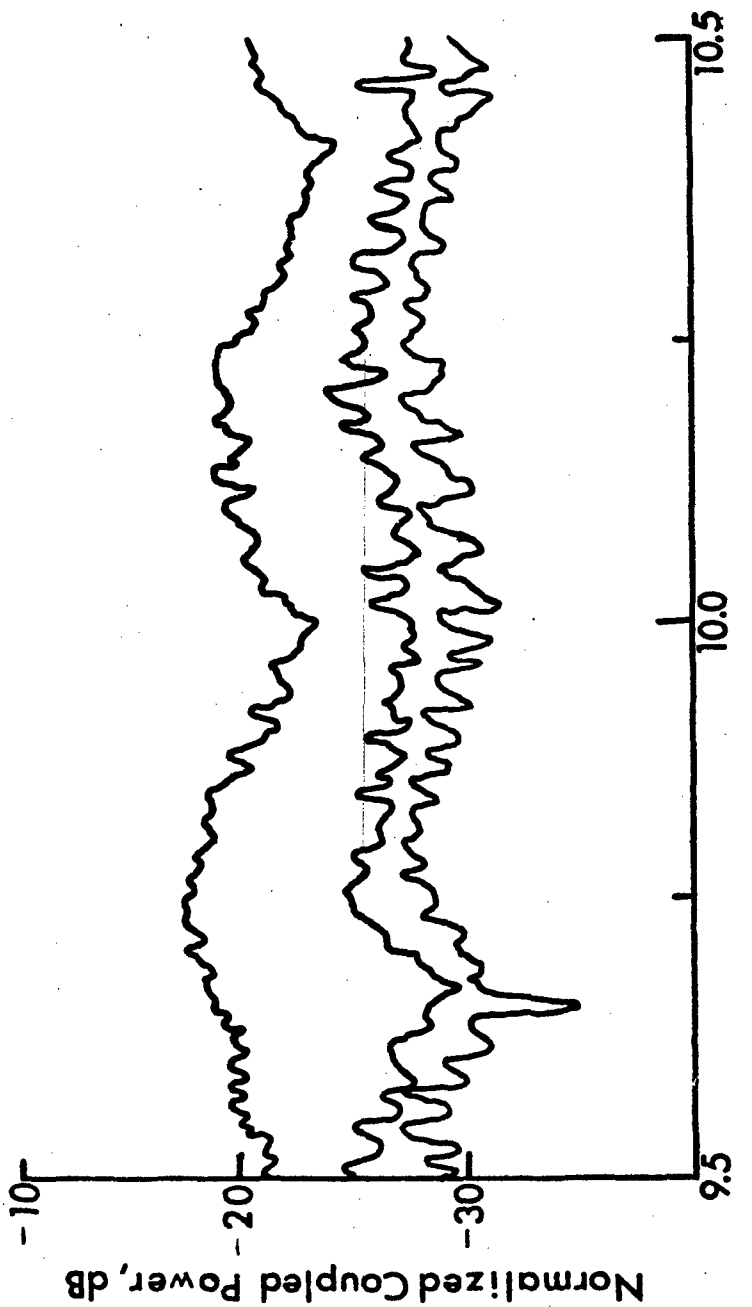

Figure 14. Typical magnitudes of coupling coefficients

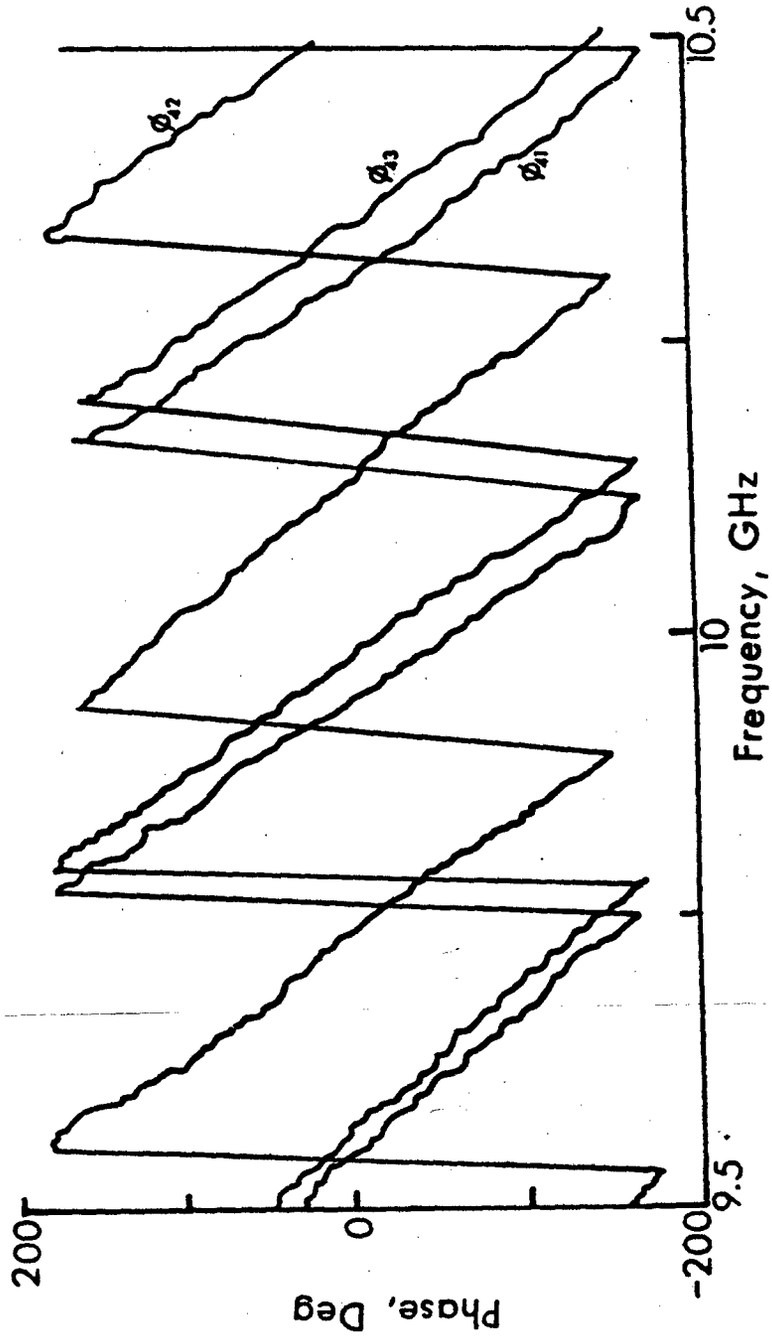

Figure 15. Typical phases of coupling coefficients

$$A_n = S_n(1+\Gamma_n) + \sum_{\substack{m=0 \\ m\neq n}}^{7} S_m C_{mn} .$$

The array factor can then be written as

$$AF(\theta) = \sum_{n=0}^{7} A_n e^{jkdn\sin\theta}$$

which is similar to Equation (1) with the desired amplitude weighting, a_n, replaced by the corrupted weighting, A_n.

Matrix algebra can be used to efficiently calculate these amplitudes through the formation of the reflection and coupling coefficients into a 2-dimensional matrix

$$[M] = \begin{bmatrix} \Gamma_0 & C_{10} & C_{20} \cdots C_{70} \\ C_{10} & \Gamma_1 & C_{21} \cdots C_{71} \\ \vdots & & \\ C_{70} & C_{71} & C_{72} \cdots \Gamma_7 \end{bmatrix}$$

Multiplying the matrix [M] by a column matrix [S] representing the input, the resulting row matrix [R] represents the total reflected signal at each element due to self-reflection and coupling from neighboring elements,

$$[R] = [M][S] .$$

The complex coefficients which contribute to the radiation pattern, can be calculated from

$$A_n = S_n + R_n . \tag{12}$$

Using (12) the array factor with the contributions from self-reflection and coupling coefficients can be calcuated for scanned beams, reduced sidelobes and other radiation patterns. Figure 16 is a computed broadside beam with uniform excitation corrupted by with the active reflection coefficients measured at 10 GHz. The coefficients were obtained from Figures 12 through 15 and similar data for the elements not shown. Figure 17 is the theoretical pattern with no errors.

Figures 18(a) and (b) are the computed active reflection coefficient corrupted patterns with amplitude tapers which ideally produce 25 and 30 dB peak sidelobe levels. A cose element pattern has been included to more accurately predict the anticipated patterns from the whole DBF array for later comparison.

A block diagram of the analog portion of the receive module which follows each elements of the array is shown in Figure 19. Critical parameters include the through phase and gain of each element which must be matched to preserve the relative amplitude and phase of the received signals. In addition, the dynamic range of the system must be considered so that none of the stages in the receiver saturate and create a nonlinear phase and amplitude response.

The first component in the receiver channel is an RF mixer used to convert the received signal to a 30 MHz IF. As discussed in Section

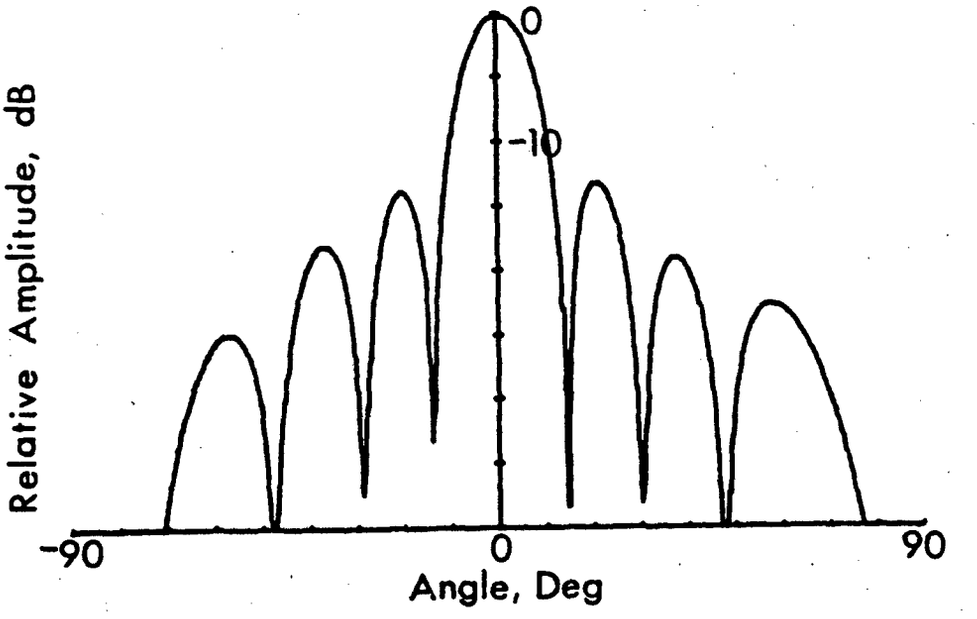

Figure 16. Broadside beam with coupling and reflection errors accounted for (.508λ element spacing)

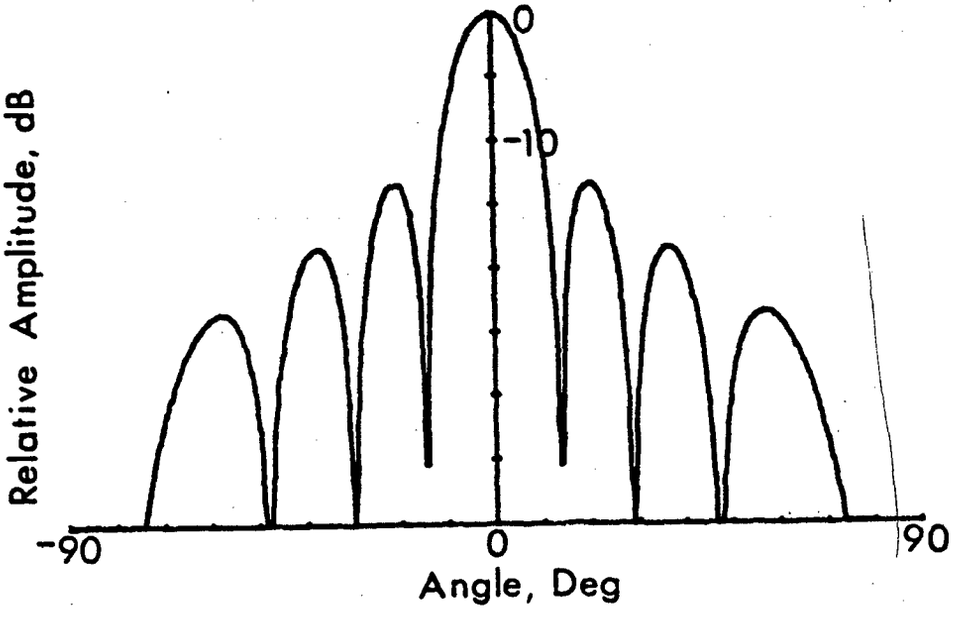

Figure 17. Ideal broadside beam (.508λ element spacing)

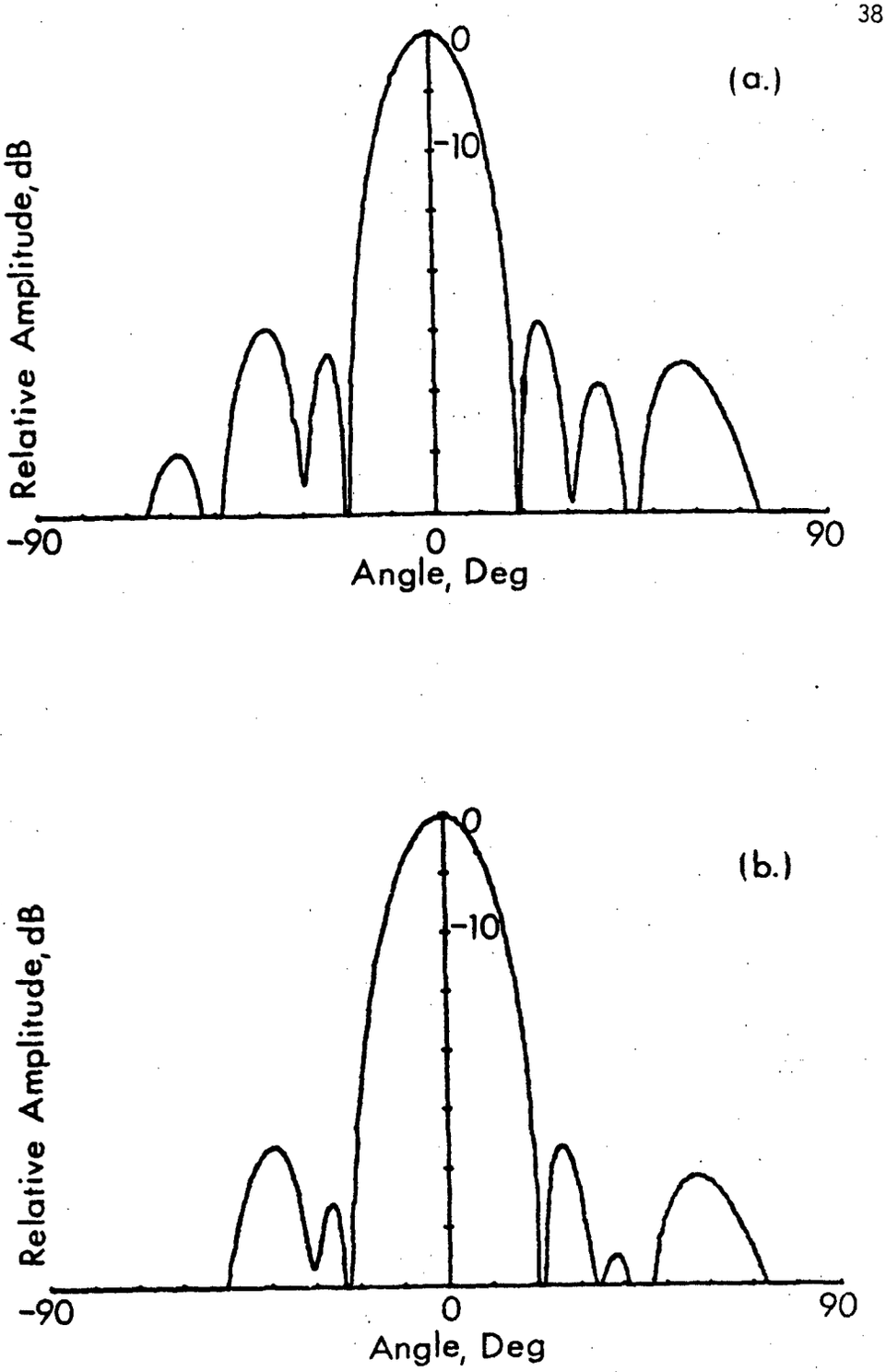

Figure 18. Antenna pattern with coupling errors and weighting for (a) 25dB and (b) 30dB sidelobes

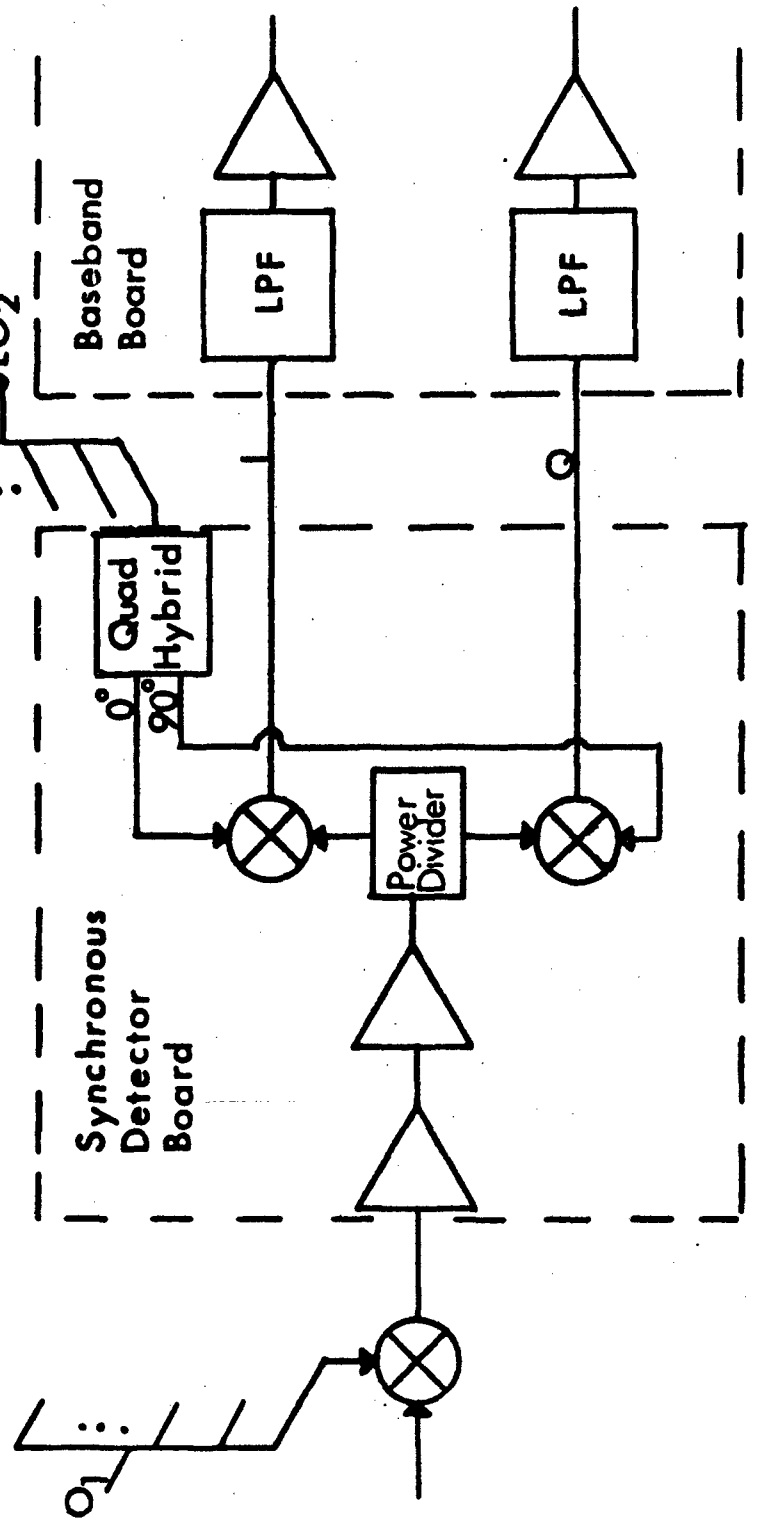

Figure 19. DBF receiver block diagram

II, the mixer output phase is dependent on the signal phase, LO phase, and insertion phase of the mixer. The relative insertion phase between the 8 mixers in each of the 8 receivers was measured at 10 GHz and is presented in Table 1. *

Table 1. Relative insertion phase of the RF mixers

Mixer Serial Number	Relative Phase
043015	0.0^{o} (ref)
043049	6.5^{o}
043027	3.0^{o}
043033	5.8^{o}
043047	4.7^{o}
043019	1.3^{o}
043035	11.3^{o}
043006	11.3^{o}

To preserve the relative phase of each element through the mixing process, the LO signals must also be matched through the LO distribution network. X-band LO distribution, called LO_1, is accomplished through use of an RF 8 way power divider with uniform phase ($\mp 8^{o}$) and amplitude ($\mp .5$ dB) response. The relative phase of the power divider output ports along with the adapters necessary to connect the mixers to the power divider were measured and the data are presented in Table 2.

* The fact that the mixers were phase matched was not a guaranteed result when the mixers were purchased. A total of 10 mixers were purchased, 7 of which were determined to be from one manufacturing lot and the other 3 from another lot. Mixers from the same lot exhibited similar phase characteristics resulting in only 7 matched mixers. During conversation with the manufacturer, he indicated that there is currently no inherent phase matching design and that obtaining matched mixers usually involved systematic measuring of the phase of many mixers to find a group with similar phase.

Table 2. Relative output phase of power divider with interconnection adapters

Power Divider Port	Relative Phase
J1	0.0^{o} (ref)
J2	$-.5^{o}$
J3	2.5^{o}
J4	-5.5^{o}
J5	6.5^{o}
J6	-14.5^{o}
J7	-8.5^{o}
J8	6.5^{o}

To get an idea of the frequency dependence of these errors, the relative phase and amplitude of the power divider ports minus the adapters were measured vs. frequency and the results are shown in Figures 20 and 21. For clarity, only the worst case amplitude error is shown in Figure 21. The figures indicate that the errors are relatively constant with respect to frequency. The next two steps in the heterodyne reception process are IF amplification followed by synchronous detection. This process is performed in a stripline board for each element as shown in Figure 19. A photo of this board is presented in Figure 22. The relative phase (referenced to the I channel of element 1, 1I) of the synchronous detector boards was measured and the data is presented in Table 3.

Since synchronous detection also includes a mixing process, another LO distribution network, called LO_2 is required. Amplitude and phase uniformity is just as necessary in this network (power divider) as it was in the LO_1 network. The relative phase of the output ports was measured and the results indicated phase differences

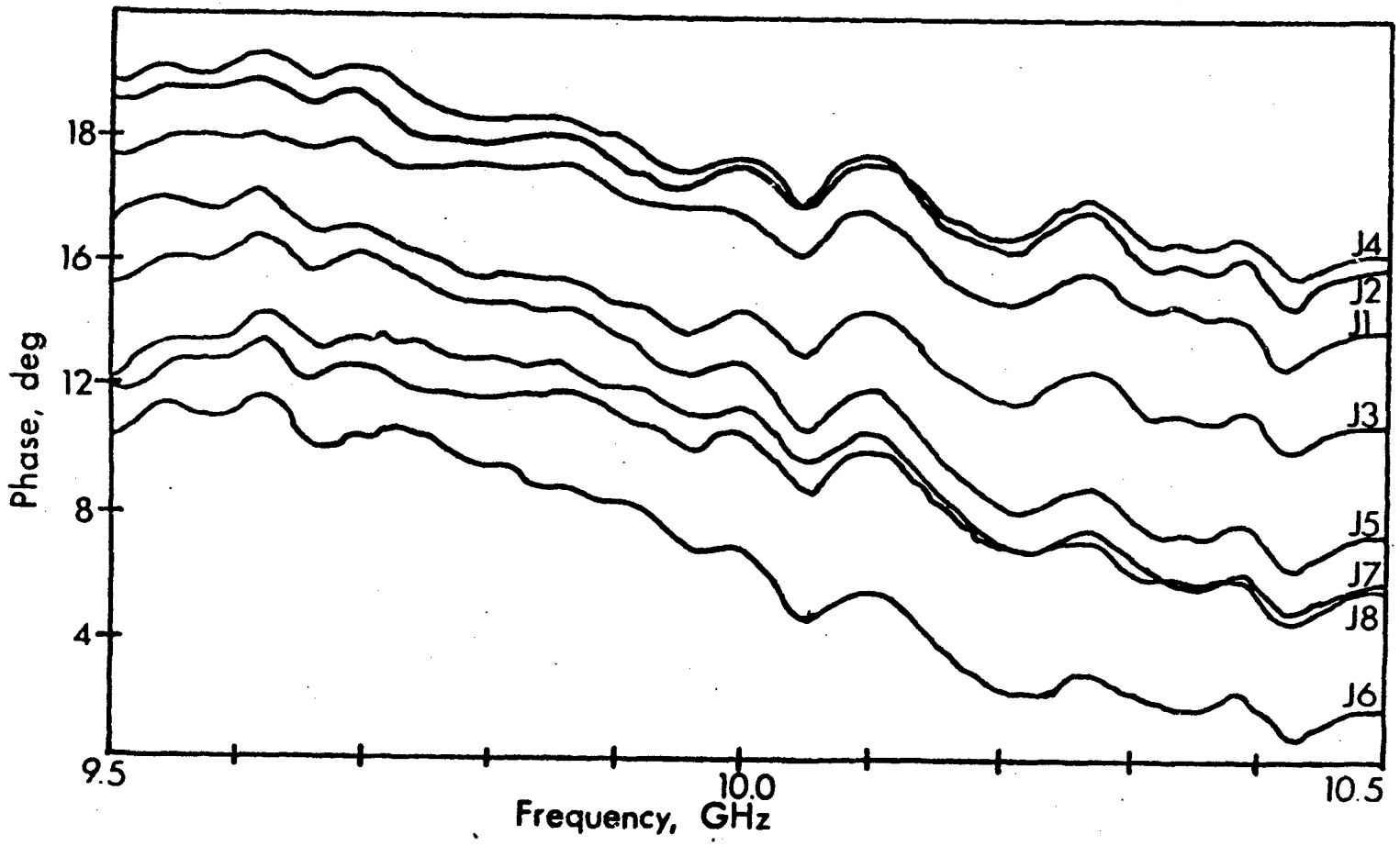

Figure 20. Phase error between power divider output ports

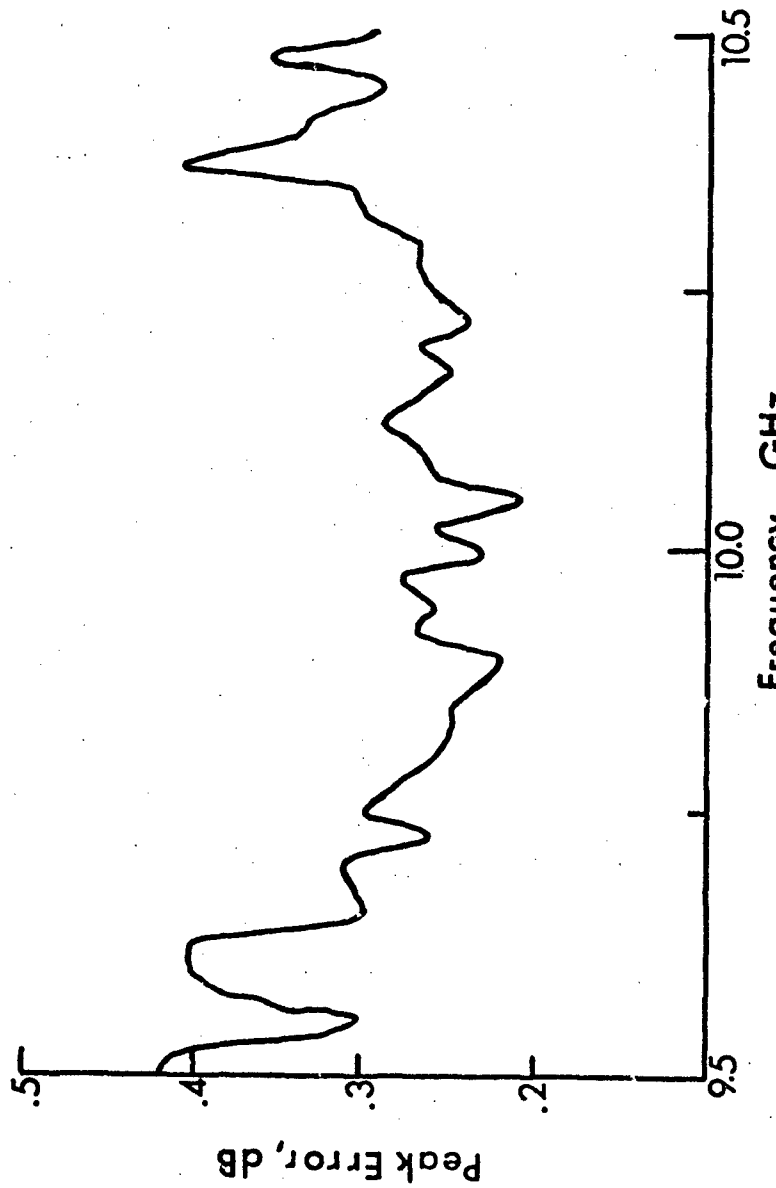

Figure 21. Peak amplitude error between power divider output ports

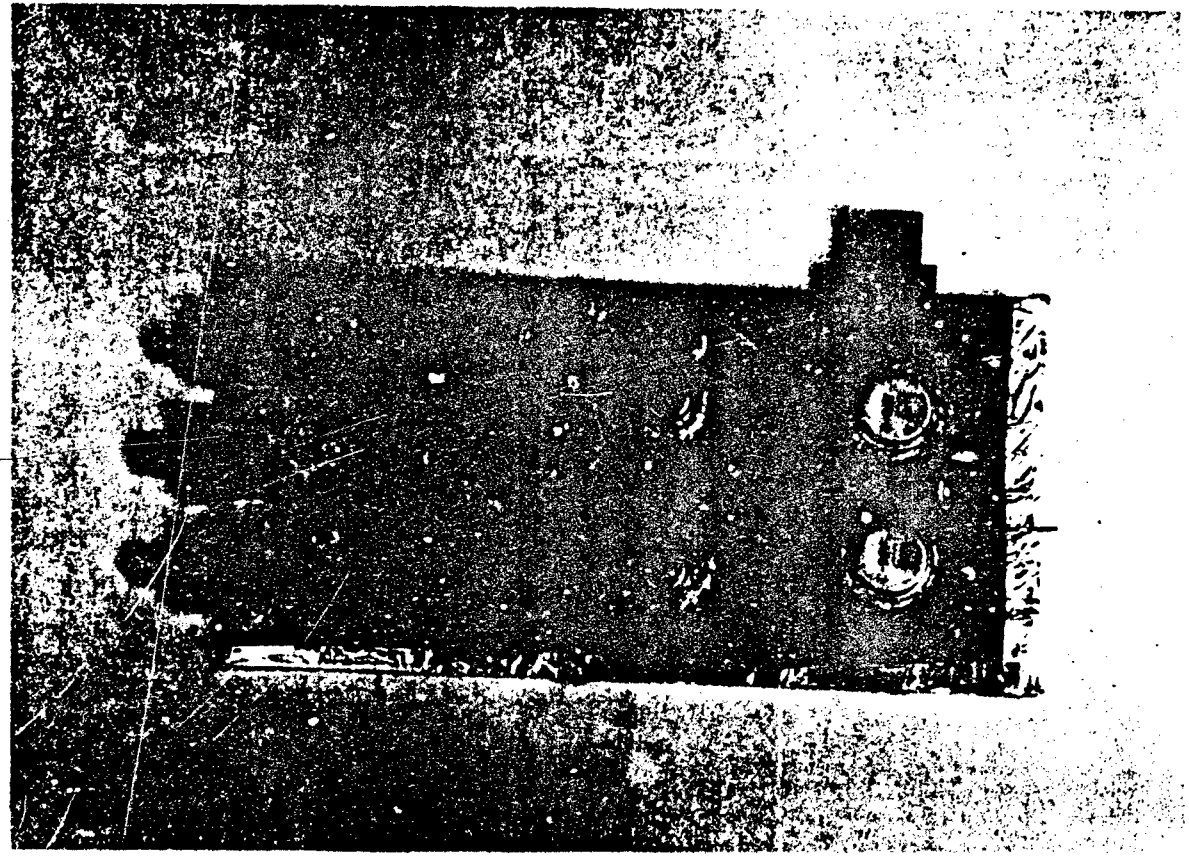

Figure 22. Synchronous detector board

less than 2^{o}. The better performance, as compared to the RF divider, is due to the lower operating frequency where the wavelengths are much longer and tolerances less stringent.

Table 3. Relative phase of synchronous detector boards

Board	Relative Phase	
	I	Q
1	0^{o} (ref)	89
2	3^{o}	93
3	6	95
4	5	92
5	5	93
6	5^{o}	95^{o}
7	6^{o}	93^{o}
8	6^{o}	93^{o}

Since synchronous detection also includes a mixing process, another LO distribution network, called LO_2 is required. Amplitude and phase uniformity is just as necessary in this network (power divider) as it was in the LO_1 network. The relative phase of the output ports was measured and the results indicated phase differences less than $\mp 2^{o}$. The better performance, as compared to the RF divider, is due to the lower operating frequency where the wavelengths are much longer and tolerances less stringent.

Table 4(a). shows each element's relative phase for the total down-conversion process. This data was taken by combining the RF mixers, LO distribution power dividers, and synchronous detector boards and measuring the output phase differences between I channels. The quadrature phase presented in Table 4 was derived from the data in Table 3.

Table 4. Relative phase of downconversion process from RF mixers through synchroncus detection; a) before compensation of element 6; b) after compensation of element 6.

Element	Relative phase I	Q	Relative phase I	Q
1	0.0	89.0	0.0	89.0
2	7.6	97.6	7.6	97.6
3	7.1	96.1	7.1	96.1
4	3.7	90.7	3.7	96.7
5	0.7	88.7	0.7	88.7
6	-11.6	78.4	3.4	93.4
7	8.0	95.0	8.0	95.0
8	8.2	95.2	8.2	95.2
	(a)		(b)	

The phase error in element 6 was larger than desired, consequently it was necessary to compensate for, or trim this error to an acceptable level. This error is essentially invariant with operating frequency, therefore, the phase trimming could have taken place almost anywhere in the element receive channel. The one care that must be exercised; however, is not to introduce a trimming method which is in itself frequency sensitive. For example, adding a line length between the antenna and the mixer would be frequency sensitive and; therefore, would not compensate for the mixer error uniformly over the operational frequency range. Since LO_2 is operated at a fixed frequency and the phase effects are reflected through the mixer, a phase compensator in this network will be invariant with frequency. Consequently, a 15^{o} phase shift was added to the path between the LO_2 divider and the quadrature hybrid servicing board #6. The final downconversion phase error associated with each element is presented in Table 4(b).

The final signal conditioning in the element receive channels is filtering and baseband amplification. In this stage, the I and Q signals are amplified to bring their levels up into the dynamic range of the A/D converter. A schematic diagram of this circuit is shown in Figure 23 and a photo of the prototype implementation is presented in Figure 24. In addition to acting as an amplifier, this section also performs needed filtering functions and amplitude gain control. Figure 25 shows a typical frequency response for the filter/amplifier combinatin. These circuits have 50 dB nominal gain and approximately a 150 kHz bandwidth. The capacitor following each stage of amplification causes the low frequency cutoff of the response. Their purpose is twofold; first they insure that a dc output offset voltage from the first stage does not saturate the succeeding stage or offset the voltage into the Track and Hold (T/H). Second, they perform some filtering of the 60 Hz line frequency. The potentiometer in the feedback loop of the first stage of amplification is used as a gain control to balance the amplitudes of all 8 elements, it provides 15dB of gain adjustment.

The phase and amplitude errors discussed thus far have varying degrees of sensitivity with respect to frequency. The errors associated with the actual antenna elements and the effects of r cual coupling vary slowly over the operating band; whereas the mixer and LO_1 power distribution related errors are virtually frequency independent. The error associated with the 30 MHz IF due to LO_2 distribution and synchronous detection are also independent of operating frequency because these devices are used only at a fixed

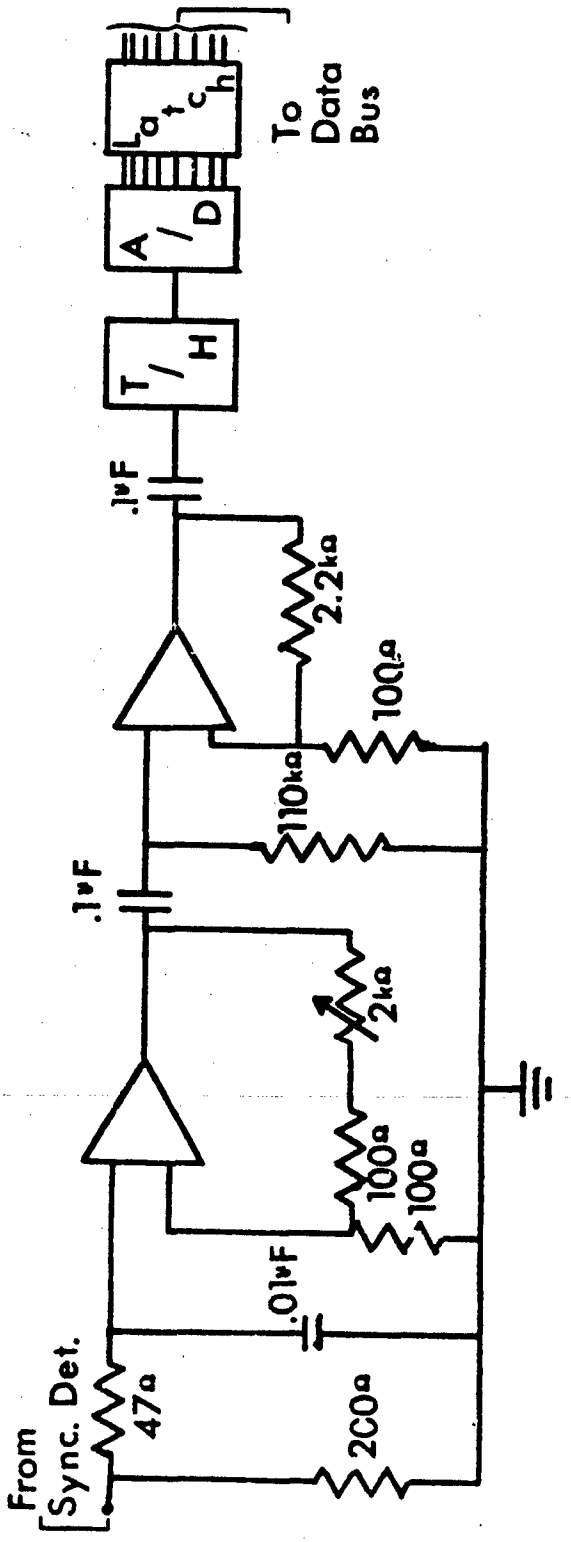

Figure 23. Baseband schematic

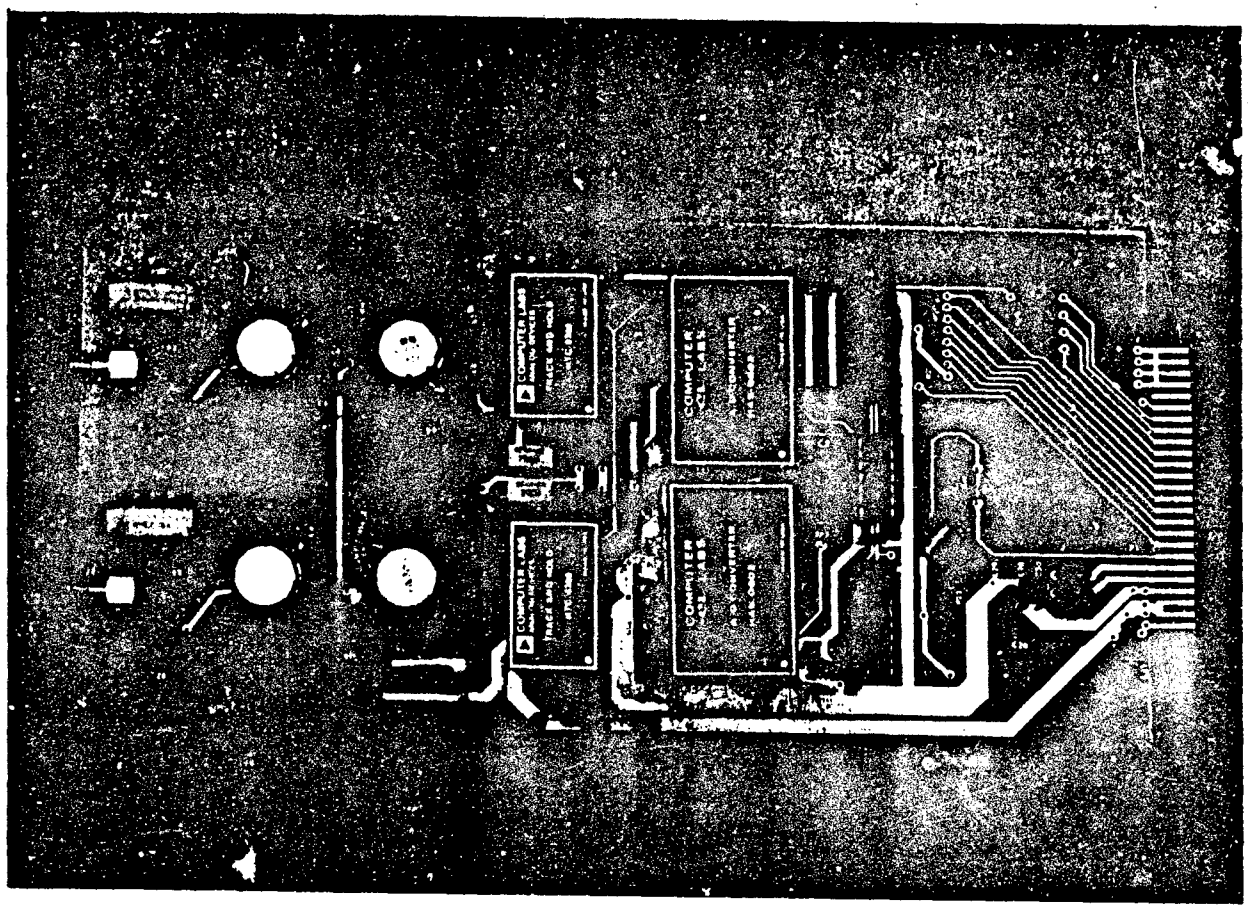

Figure 24. Baseband board

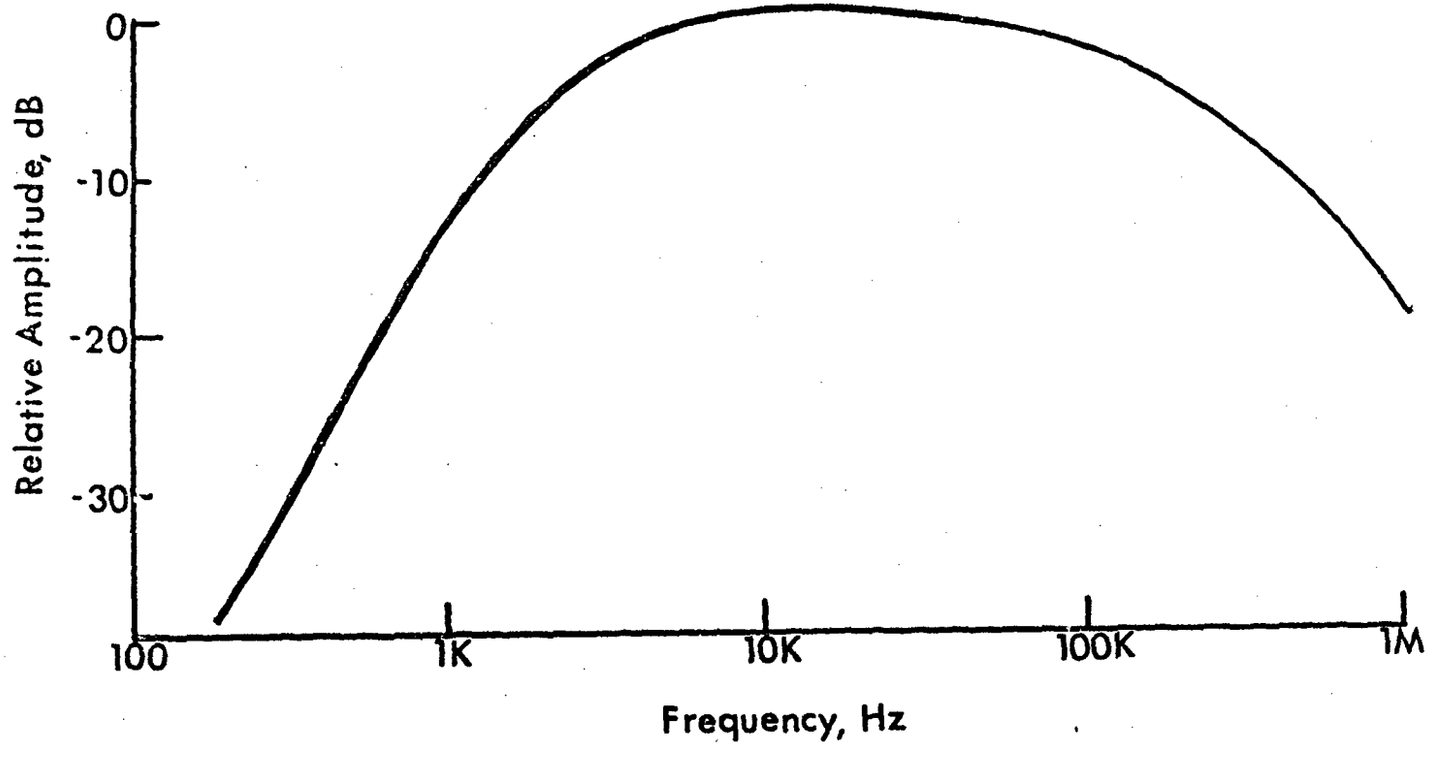

Figure 25. Frequency response of filter/amplifier combination

frequency. Consequently, from initial reception through synchronous detection the errors are fixed once the operating frequency is selected. This would also be true through baseband filtering and amplification if the signal were at a single frequency or contained in a very narrow spectrum. However, in order to maximize signal to noise ratio the final baseband amplifier is given a bandwidth as narrow as possible while still preserving information content (matched filter). The result of this process is to have phase and amplitude errors which vary over the systems signal bandwidth. This effect is most pronounced near the band edges where component tolerance effects are most strongly exhibited.

For example, as shown in Figure 26, the phase response of a single pole high pass filter changes at a rate of 45^{o}/decade between $.1f_c$ and $10f_c$, where f_c is the 3dB point or breakpoint of the filter. This means that in the first decade of the passband the through phase varies with frequency. For two networks having identical breakpoints, this does not cause a problem in matching because the through phase for the two networks would be equivalent even though it would be changing between f_c and $10f_c$. However, variations in the breakpoint produce a horizontal shift of the curve which causes two networks having slightly different breakpoints to have a different through phase between the frequencies f_c and $10f_c$. At frequencies much above $10f_c$, the relative phase remains constant. For networks having more than one breakpoint, the response becomes the sum of the individual responses.

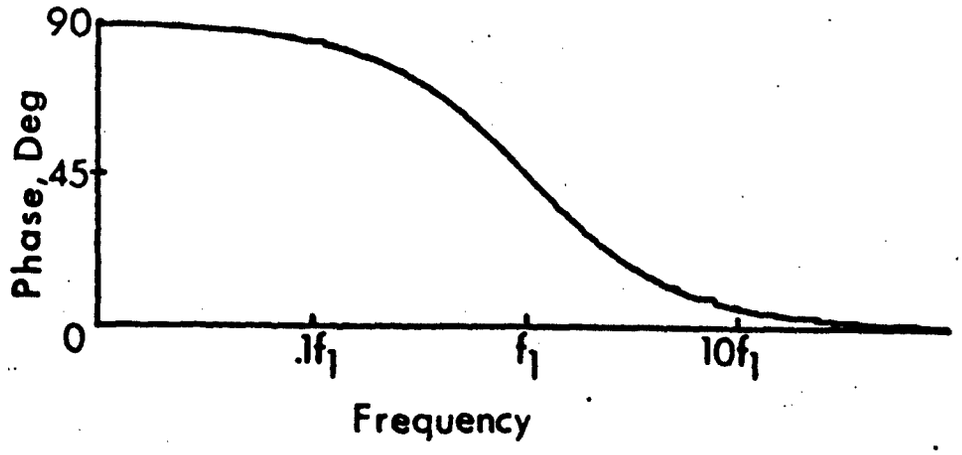

Figure 26. Phase reponse of single pole high pass filter.

From Figure 25, the filter/amplifier pair has a low pass breakpoint at 3 kHz and a high pass breakpoint at about 150 kHz. The phase response can be characterized given these two breakpoints and is shown in Figure 27 along with the response of a network with a 20% variation in the capacitor contributing to the high pass characteristics. There is no range of constant phase shift and component variations between two networks will cause the through phase of the network to be different as shown in the figure. The response of the antenna pattern is therefore dependent on the frequency of the receive signals when the baseband networks are not matched.

From Figure 27, it is apparent that the maximum error will occur at frequencies corresponding to the maximum slope along the curve. This was verified by a measuring several baseband boards in the frequency band of interest and determining an average error at several frequencies. This data is presented in Table 5.

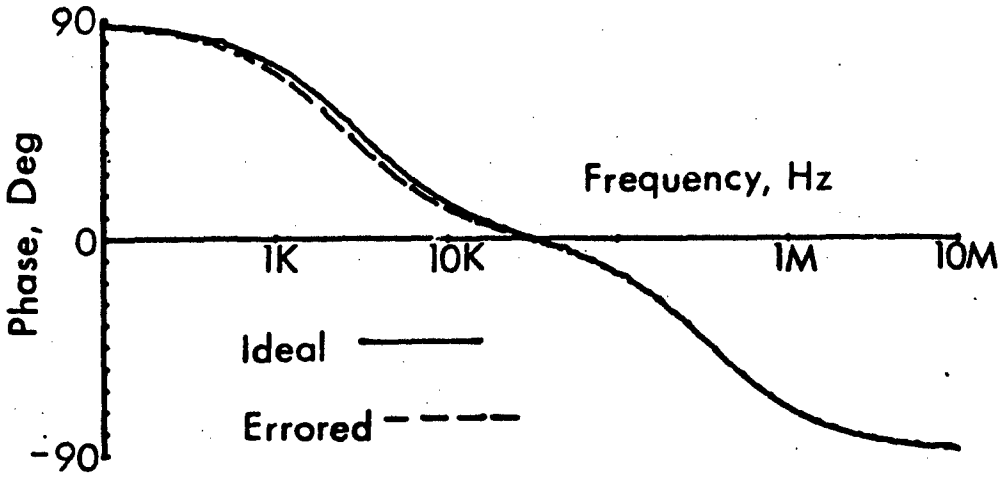

Figure 27. Phase response of filter-amplifier combination.

Table 5. Peak-to-Peak phase error vs. frequency in baseband boards.

Frequency Hz	Phase Error, deg
1K	3.5
2K	3.5
5K	2.5
10K	1.5
20K	1.0

The effect of the I to Q errors after digital conversion is somewhat different than the errors discussed previously, not only because of the frequency dependence but also because of a time dependence. Although the actual phase error between I and Q in an element remains essentially constant with respect to time at a frequency, the

effective error will vary between time samples and the subsequent calculation of the phase, ψ, using the arctangent function. Ideally, the I and Q signals can be written as two signals equal in amplitude and separated by 90^0 in phase. Error effects can be included by introducing different amplitudes, K_1 and K_2, as well as a lumped phase term representing the phase error relative to an arbitrary reference phase. The two errored signals can be written as

$$I = K_1\cos(\omega_d t+\delta_1)$$

$$Q = K_2\sin(\omega_d t+\delta_2)\,.$$

The gain control in the baseband amplifiers sets $K_1 = K_2$. For an ideal I and Q signal, $\delta_1 = \delta_2 = 0$, and the phase calculated from Equation (8) is

$$\begin{aligned}\phi &= \tan^{-1}[\sin(\omega_d t)/\cos(\omega_d t)]\\ &= \tan^{-1}[\tan(\omega_d t)]\end{aligned}$$

Now if $\delta_1 \neq \delta_2$ the errored phase denoted by ϕ' is

$$\phi' = \tan^{-1}[\sin(\omega_d t+\delta_2)/\cos(\omega_d t+\delta_1)]\,.$$

The phase error, E, is then given by

$$\begin{aligned}E &= \phi-\phi'\\ &= \omega_d t-\tan^{-1}[\sin(\omega_d t+\delta_2)/\cos(\omega_d t+\delta_1)]\end{aligned} \qquad (13)$$

where ϕ is the correct phase and δ_1 and δ_2 are the errors in the I and Q channels respectively relative to a reference phase. For small errors, δ_1 and δ_2 less than 20^0, the effective error varies almost

sinusoidally and (13) can then be approximated by

$$E = \frac{-(\delta_1+\delta_2)}{2} + \frac{(\delta_1-\delta_2)}{2}\cos(2\phi). \qquad (14)$$

Figure 28 is a graph of the effective error as a function of phase for both the actual (13) and the approximate (14) formulations.

Since the phase of the signal varies from sample to sample, the effective error will also vary with every sample. Assuming the sampled phase varies uniformly from 0 to 360^0 and that the corresponding error varies sinusoidally, the effect of the error on the antenna patterns can be simulated. Figure 29 shows the effect of a 2.0^0 rms error between I and Q channels of each element on the antenna pattern of Figure 18(b).

Following the amplifiers, a T/H (Analog Devices HTC0300) is used to present the A/D converter a fixed voltage for digitizing. A fixed level is necessary to reduce errors caused by signal variation during the A/D conversion time. The A/D converter used in the prototype array is an 8 bit device with an input range of $\pm$ 5.12V, which results in 40mv between least significant bit (LSB) states. It is a successive approximation type which compares the current analog input to the analog equivalent of the most current digital output. On the rising edge of the ENCODE pulse the outputs are cleared, then on the falling edge the comparison process begins. Beginning with the most significant bit (MSB), each bit is set high and a comparison to the input is made. If the input is less than the voltage equivalent of the digital output, the bit is cleared. If not, the bit remains high and the next

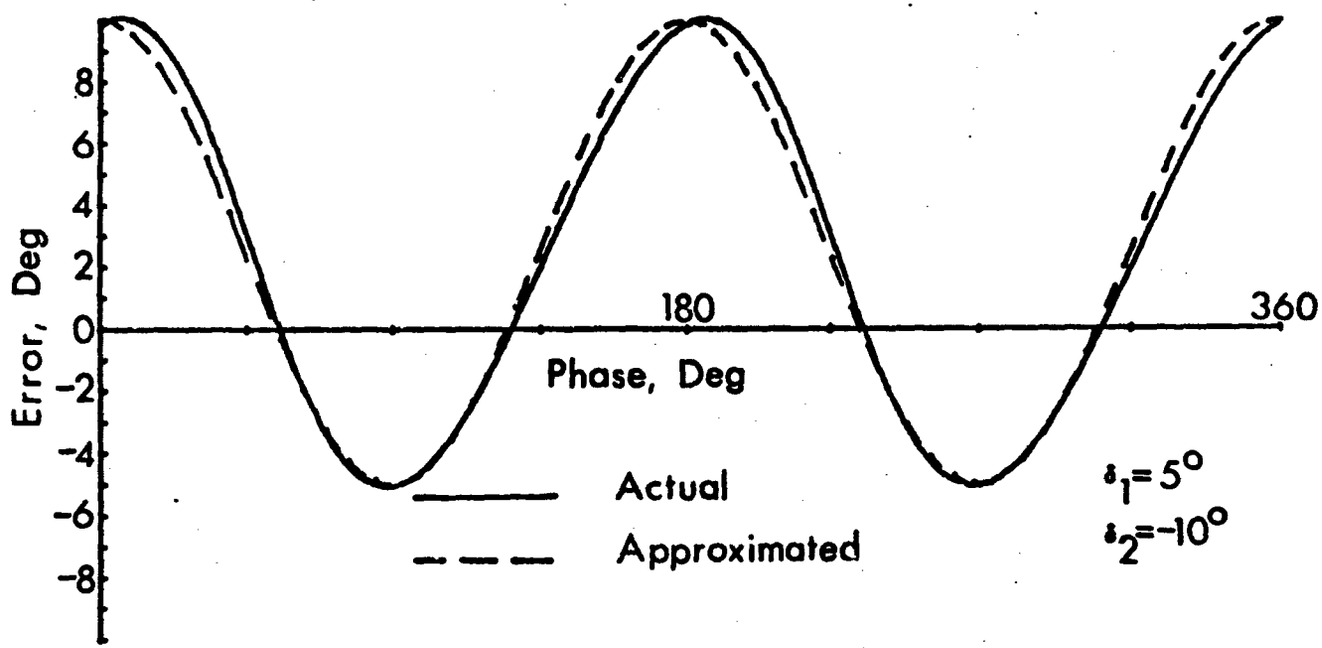

Figure 28. Phase error vs phase angle for digitized baseband signal

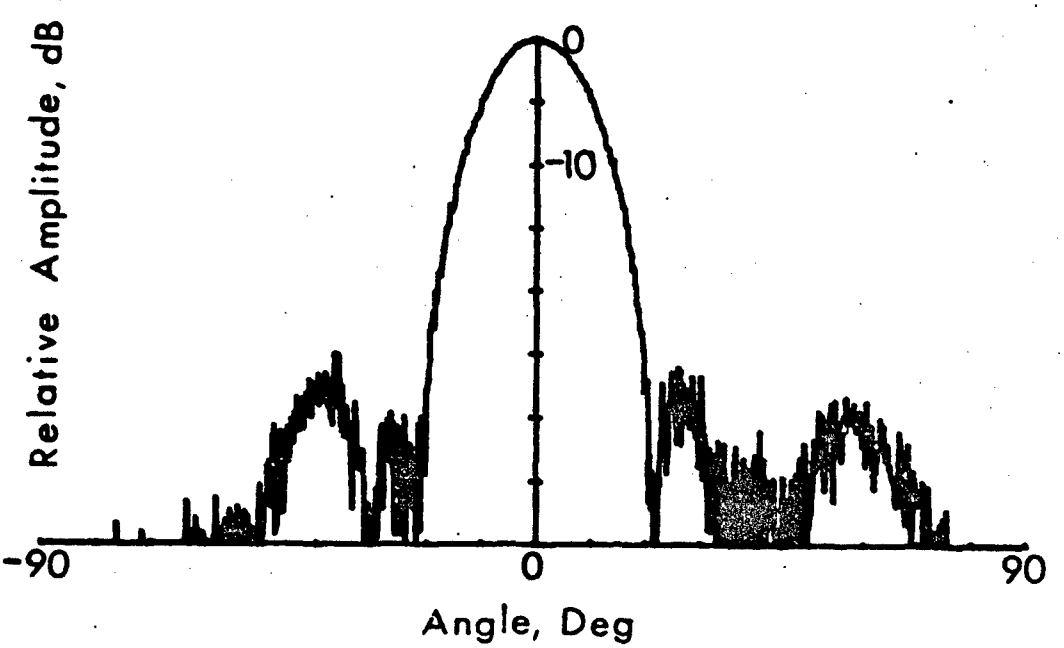

Figure 29. Simulated antenna pattern with coupling errors and 2° rms I and Q errors

bit is set and again the input is compared to the new digital word. This continues until all 8 bits have been tested. The resulting bit pattern represents the input signal.

When converting a time varying signal it is possible that between the time the ENCODE command is received and digital conversion is complete (1.2μsec), the input signal may change by more than 1 LSB. For example, if a 5 volt 10 kHz sinusoid is applied to the A/D converter directly the variation in amplitude during the conversion time could be as much as 0.37V depending on the point where the waveform is sampled. In this case the signal is given by

$$s(t) = 5\sin(20{,}000\pi t)$$

and the slope or signal variation is a maximum when

$$\frac{d^2s}{dt^2} = 0 = 5(20{,}000\pi)^2 \sin(20{,}000\pi t).$$

Solving for t, yields

$$t = n/20{,}000\pi t \quad n = 0, 1, 2, \ldots$$

The signal variation at this worst case point is the conversion time, t_c, multiplied by the slope of s(t) at t = 0, or

$$\begin{aligned} \Delta s &= t_c \frac{ds}{dt} \\ &= (1.2 \times 10^{-6})(.5)(20000\pi)\cos(20000\pi t)\Big|_{t=0} \\ &= 0.37 \quad V . \end{aligned}$$

Since the LSB of the A/D is 40mV, the 0.37V variation results in as much as a 10 LSB error in conversion.

When the T/H is used and all the T/H devices are enabled simultaneously the error is reduced significantly. The T/H has an aperture uncertainty* of 100 psec which will result in an amplitude variation no greater than

$$\Delta s = t_c \frac{ds}{dt}$$

$$= (100 \times 10^{-12})(.5)(20000\pi)\cos(20000\pi t)\Big|_{t=0}$$

$$= 3.1 \times 10^{-6} \text{ V}$$

for the maximum voltage input. This voltage level is substantially less than 1 LSB. Another important parameter of the T/H is the droop or discharge rate of the HOLD capacitor.

Droop effect in a T/H are worst when the voltage to be held is high. Measurements showed the droop rate to be less than 4 μV/μsec with a 5V input signal. The worst case droop of 4 μV/μsec results in a change of 4 μV/μsec times 1.5 μsec or 6 μV during the conversion time of the A/D. This is negligible in terms of the 40mV LSB.

The selection of the 8 bit Analog Devices HAS-0802 A/D convertor was based on obtaining an off-the-shelf A/D with relatively simple interface requirements, having a moderate dynamic range (7 bits + sign = 42 dB), and a conversion time fast enough to sample a radar waveform

*Aperture uncertainty is the unit-to-unit variation between when the HOLD command is applied and when the internal gate opens.

capable of 300 m range resolution.* In the context of this antenna report, the conversion time of the A/D is not critical, being limited ultimately by the droop rate of the T/H. However, upon completion of the antenna tests, the hardware is to be modified to perform a radar function dictating the need for a relatively fast conversion time.

There are two types of A/D errors, quantization and linearity. Quantization errors are inherent in an A/D because the converter approximates an analog signal with a discrete digital word. The quantization error is determined by calculating the variance (power) of the distribution function over an interval of 1LSB. Taking the interval about analog "zero" and letting q = 1LSB, the variance is

$$\sigma^2 = \int_{-q/2}^{q/2} x^2 p(x)dx \quad = q^2/12 \qquad (15)$$

where the probability density function is uniform between -q/2 and q/2 and has a value of 1/q. The quantization error in terms of noise voltage is then $40/\sqrt{12}$ or 11.6 mV, based on the 40mV LSB. The maximum signal to noise level that can be obtained for a full scale input voltage is

$$S/N = 10 \log \left[\frac{v^2/2}{\sigma^2}\right]$$

---

* The range resolution cell size, r, can be no smaller than

$$r = \frac{ct_c}{2} = \frac{3\times10^8 \times 1.2\times10^{-6}}{2} = 180m,$$

based on the A/D characteristics. Pulse width also affects the range cell size.

$$= 10 \log \left[\frac{5.12^2/2}{.0116^2} \right]$$

$$= 49.92 \text{ dB} .$$

The second source of A/D errors can be broadly classed into a term called linearity errors [16]. Linearity is a measure of the variation in the difference in input voltage necessary to change the output of the A/D. Put more simply, linearity is the variation of the LSB between different digital states. There are two types of linearity errors, the first is a random error, bit state to bit state, its effect is similiar to a raised noise floor. The second type of linearity error is a systematic error in the adjacent LSBs. For example, many A/D's exhibit a variation in LSBs which is quadratic such that the LSB at the higher levels is larger than the LSB at the low conversion levels. The result of systematic linearity errors, is the creation of harmonic responses in a frequency or spatial transform process.

One method to characterize the linearity errors in an A/D convertor is to digitize a known sinusodial waveform and perform a Discrete Fourier Transform (DFT) on the digital output. The HAS-0802 devices were put into a test setup which performed a 1024 point real DFT weighted with a 100 dB Chebyshev function. The output of each filter from an ideal 8 bit A/D converter is shown in Figure 30. Only the responses of filters 20 thru 511 are plotted, to avoid the dc response and because the response is mirrored in filters 512-1024 in a real DFT. Theoretically the noise floor is at -49.92 dB and this value is

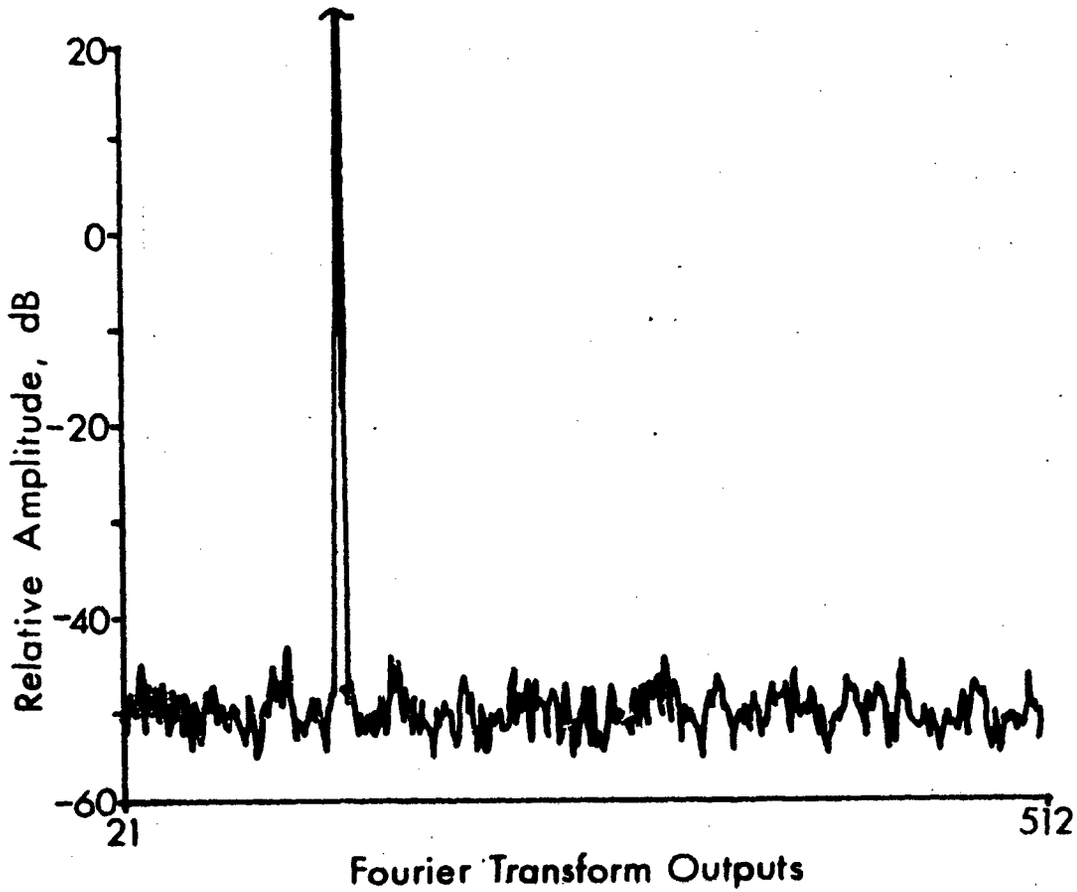

Figure 30. DFT response to an ideal A/D. Ordinate is relative amplitude with respect to a 5.12V peak sinusoid input to DFT

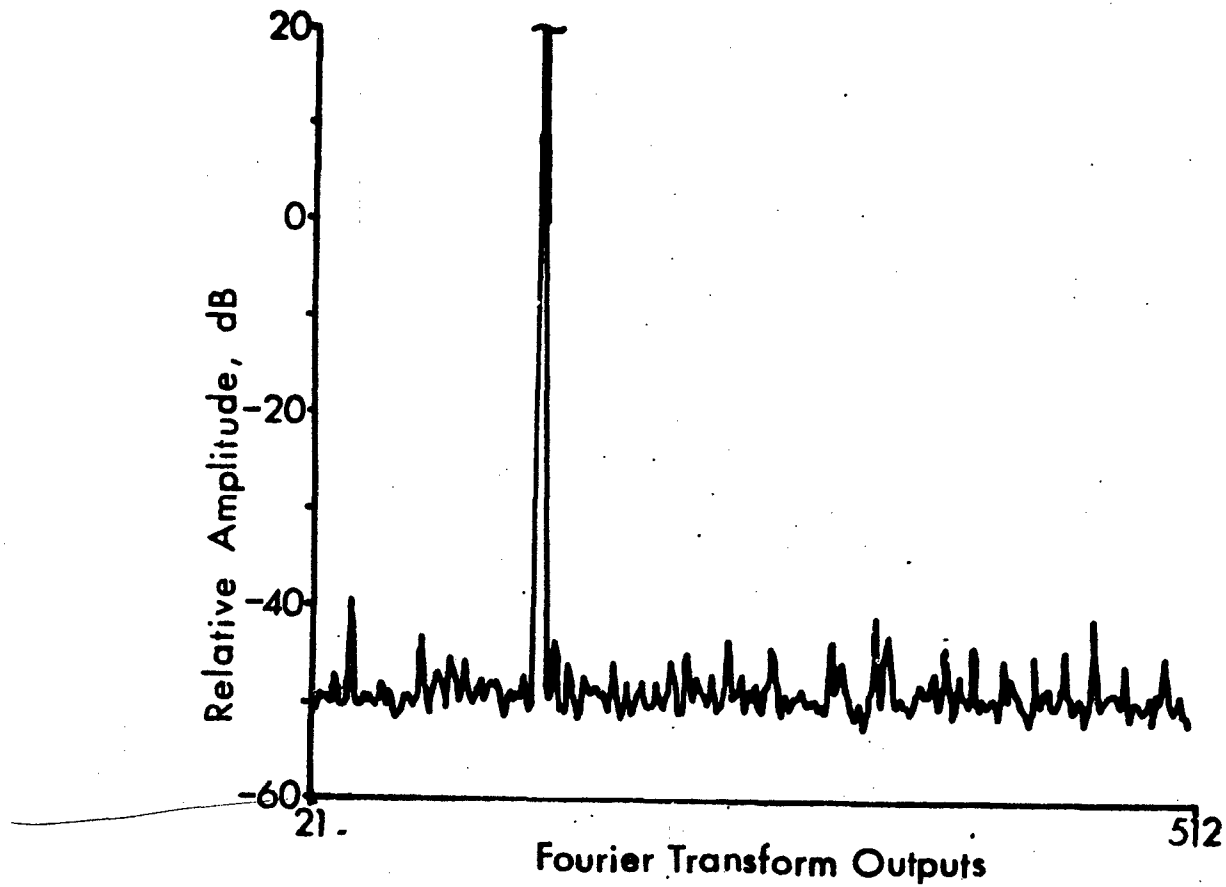

Figure 31. DFT response for a typical HAS-0802 A/D. (Ordinate is same as in Figure 34 but actual input is 3V peak to A/D converter)

verified in the noise level shown in Figure 30. The response of a typical HAS-0802 A/D to a 3V peak sinusoid is shown in Figure 31. Two effects are noticed when compared to the ideal A/D. There is a slight rise in the overall noise level accompained by some non-noise like spikes caused by harmonic distortion. The A/D average noise floor is at -48.5 dB with respect to a full scale input signal. This raised noise floor is due to random and linearity errors and represents a 1.5 dB average loss when compared to the ideal A/D. This error can be related to antenna performance directly. The A/D noise floor is in effect the lowest sidelobe level, with respect to isotropic, that can be obtained with the array. However, from the previous antenna array measurements, it was shown that due to the array itself, sidelobe suppression of only about 25 dB is possible and therefore the A/D errors are negligible for these antenna tests when compared to the other errors if a sufficient signal level is applied to the A/D. The signal level necessary to assure that the peak of the mainbeam is at least 40dB above the A/D noise is calculated from

$$-48.5 + 40 = 20 \log(E/5.12)+G_i$$

where E is the peak signal voltage and G_i is the integration gain (9 dB) of the 8 point complex DFT to be used in this system. Solving for E, the minimum signal level is .68 V peak.

Throughout this section only the phase errors have been discussed at any length; generally these errors are not only much more critical to array performance, but also are more difficult to control than amplitude errors. In the prototype system a gain control was put into

the first stage of baseband amplification, in order to balance the gain variations in the receive circuitry. This location was selected because the errors occurring in the track and hold and A/D conversion were very small and have very little effect on the antenna's performance. The actual gain settings were made by placing a source near broadside in the far field and equalizing the I and Q rms voltage in each element. This technique will account for all amplitude imbalances caused by the down-conversion and final amplification process, as well as any amplitude imbalances in the antenna aperture due to mutual coupling effects at broadside. Coupling differences due to illumination functions variation and scanning cannot be compensated for in this array. Moreover, this amplitude calibration approach assumes an equal amplitude wave across the aperture, which may not be the case if multipath is present or if the source is not in the far field. If either of these conditions exist they will be compensated for and therefore cause an illumination function error when the antenna is moved to a different position.

IV. ANTENNA PATTERN DATA

Upon assembly of the complete array described in the previous section, antenna pattern data was taken to establish performance bounds and relate component error effects to pattern characteristics. In a DBF array several features require that a somewhat unconventional approach be taken toward both data gathering and data reduction. For example, a conventional antenna pattern is taken by recording, typically on chart paper, the output of a single beam port as a function of angle. However, in the DBF array all element outputs are sampled as a function of angle and the actual pattern is formed afterward. The pattern is not unique in that the same data can be weighted in many ways in the computer depending upon the desired purpose. This feature was used as a data reduction and analysis tool in order to form different types of beams to accentuate different error effects.

A block diagram of the equipment and interfaces used to take antenna patterns is shown in Figure 32 and a photograph is shown in Figure 33. The transmit signal (10 GHz) is derived from mixing LO_1 and a stable 30.010 MHz source. This combined signal, after appropriate filtering and amplification, was transmitted from a remote source, received, and down-converted to 0.010 MHz or 10 kHz at each element. This offset is necessary for the signal to pass through the baseband amplifiers. The actual transmit horn was mounted on a tower 31 feet away from the receive array. This easily satisfies the far field criteria for pattern measurements of $2D^2/\lambda$ which is slightly over 5 feet at X-Band. Because of the pattern range geometery, it was

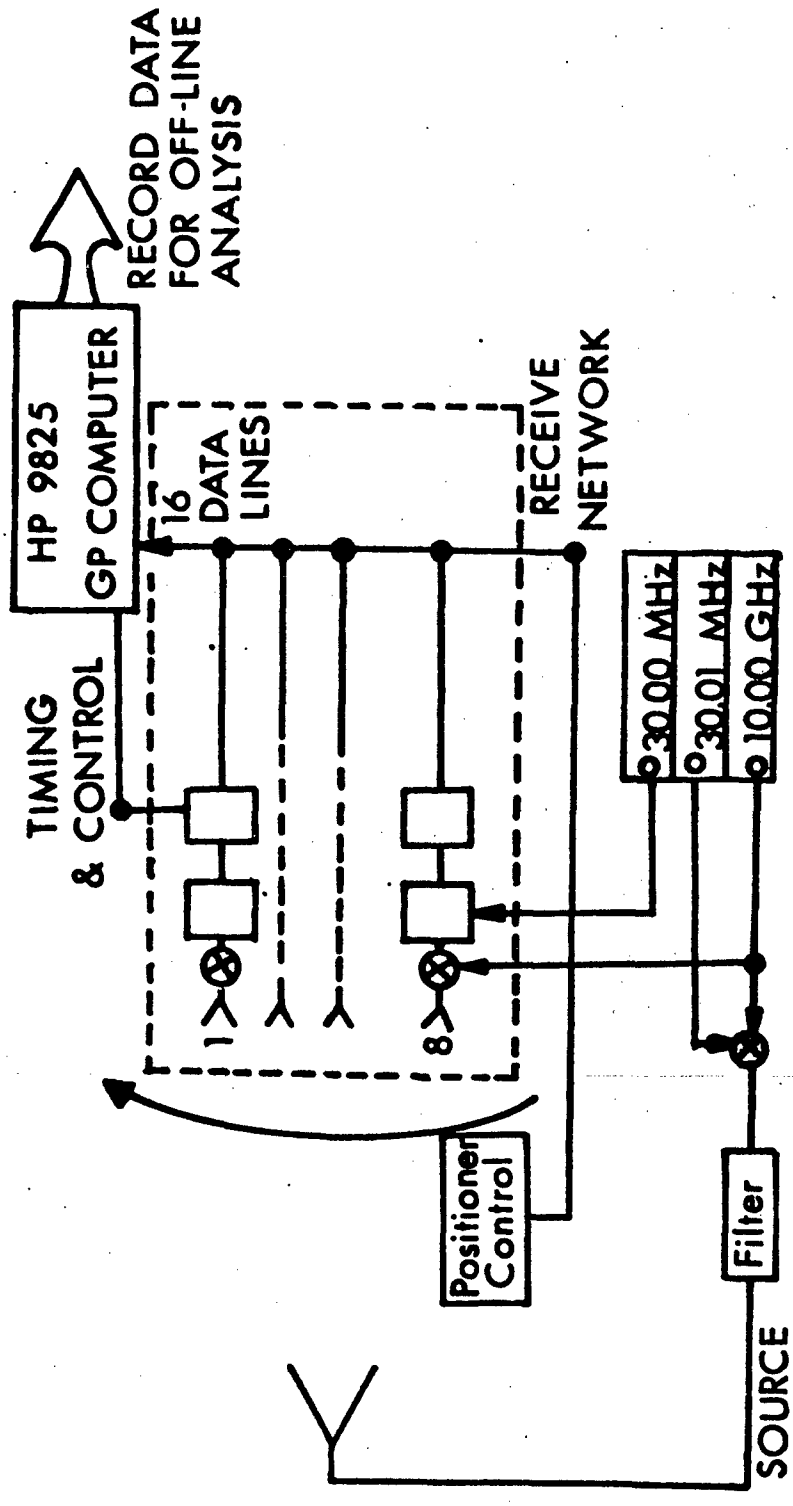

Figure 32. Block diagram of equipment layout

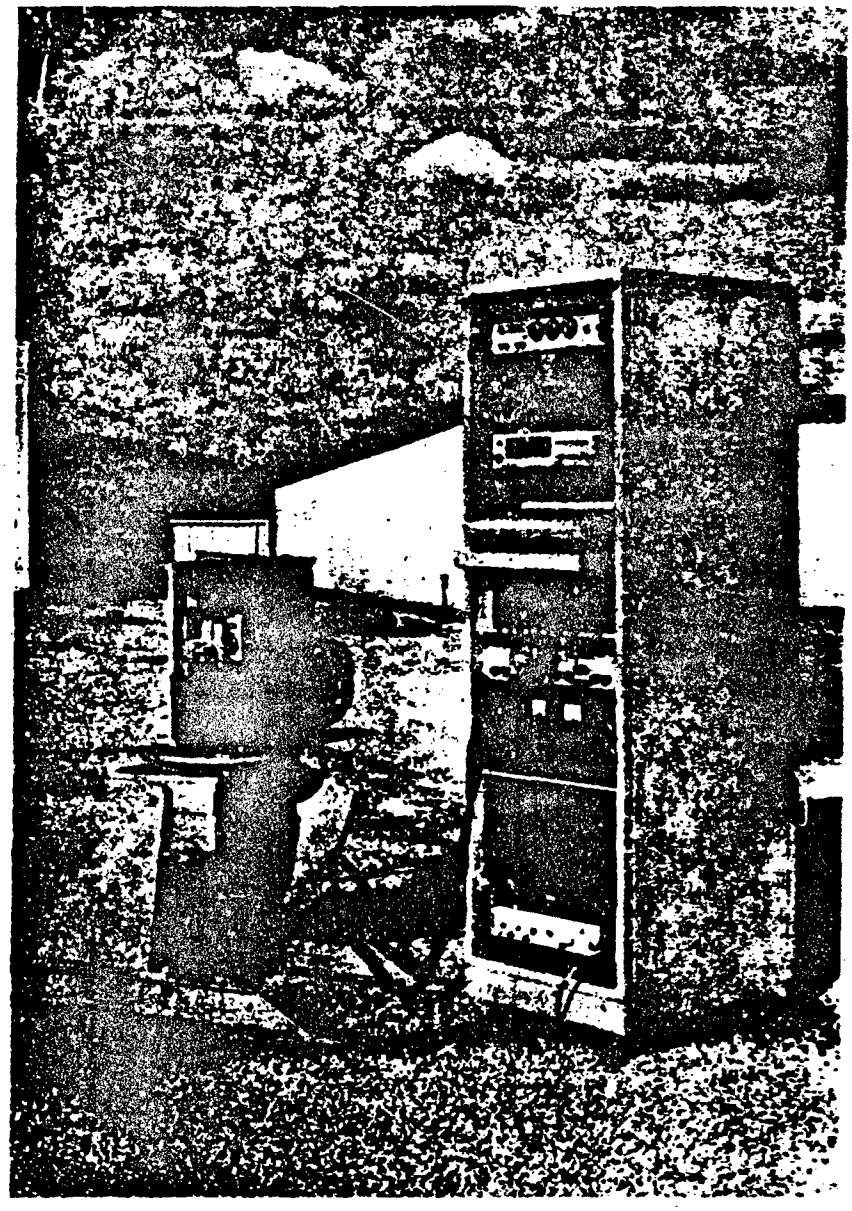

Figure 33. Equipment setup for pattern test

necessary to rotate the array 90^0 to avoid pattern variations due to multipath. With this modification the 180^0 of elevation angle scan was obtained by rotating the positioner about its azimuth axis which avoided pointing the array at the ground during the tests.

To determine the angle at which each set of data was taken, a 12-bit synchro to digital (S/D) converter (Analog Devices SDC 1725622) was used to digitize the angle indicated by the antenna positioner. The three synchro and two reference signals from the antenna pedestal, which normally feed the chart motor in the pattern recording equipment, were the inputs to the S/D converter.

The dynamic range of the receive signal was controlled by a combination of adjustments to the transmit signal and the gain control in the baseband amplifiers. Between these two adjustments it was possible to get the maximum received signals to within 2.6 dB of the maximum allowable A/D signal while the thermal noise was approximately 10 dB below the A/D LSB. In order to balance the system, the receive array was pointed at the elevated transmit horn and the elements were balanced in amplitude through the variable gain stage of the baseband amplifiers. As mentioned earlier, the "balancing" may not account for small variations in gain through all receivers due to the coupling and multipath. It does, however, provide a method of reducing variations over time.

A Hewlett Packard 9825 Calculator was used both as a controller and a data acquisition system for the pattern tests. The calculator was connected to the array through a 16-bit interface cable (HP 98032). This interface cable is capable of providing control signals

to activate the Track and Hold circuits, A/D convertors, and tri-state latches. The interface also has input capability for 16 bits, which are divided into two 8-bit words representing each elements I and Q signal. The angle data from the positioner synchro is input to the calculator in the same format as the element I and Q data. The digital output of the synchro has only 12 bits* so the four LSB's of the 16 that are stored for position are not used.

The software was written for the HP 9825 so that the computer was writing commands to the array while reading the antenna position continuously. When the positioner indicated a .2637^{o} change (3 LSB's) in position, the computer would store a new set of I and Q data and the angle at which the data was taken. In this way, with the positioner running slowly, the data was taken at intervals of .2637^{o} which for the 180^{o} sweep results in about 680 position points. A flow diagram is shown in Figure 34. After storing the element and position data from a 180^{o} sweep of the positioner the data was recorded on magnetic tape for later processing.

Once the position and element output data was recorded the data analysis could be performed. Since the data was stored on tape through the use of the HP 9825 calculator, it was very easy to use the 9825 for data reduction also. Two general classes of programs were written to analyze the data. The first type was a group of programs which examine the elemental data to see if it is valid or to specifically examine element-to-element signal characteristics. The second

*12 bits of angular information results in a resolution of .0879^{o}

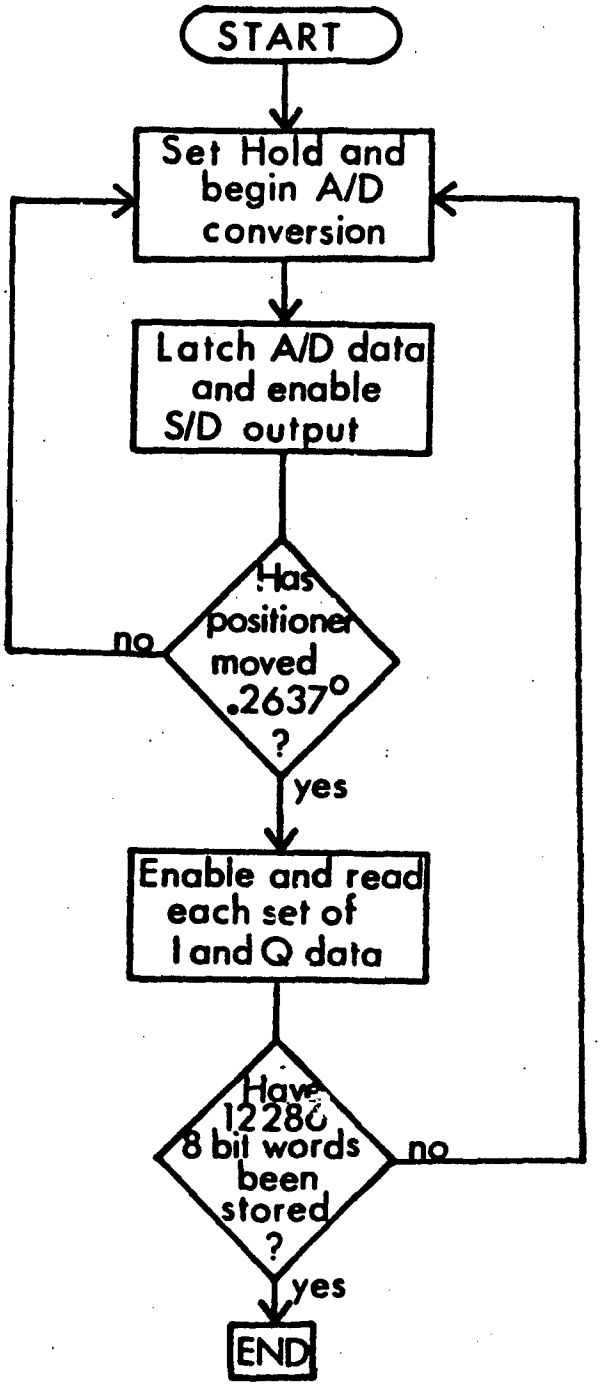

Figure 34. Computer flow diagram

type of programs were developed to form patterns with combined element data, just as a DBF spatial processor would do.

The most useful analysis performed on the individual element data was the computation of phase and amplitude errors. The phase errors are computed by applying a least squares fit to the linear phase front across the array. The difference between the least squares line and the calculated phase at an element is defined to be the error at that element. This is not an absolute error because the least squares line does not represent the actual phase slope, only an approximation with respect to the data. The amplitude errors are found by computing the average magnitude across the array and comparing each element's magnitude to this average. Ideally, these errors should be small; however, the amplitudes were balanced with respect to broadside coupling so that as the antenna is rotated and coupling changes, the elements are no longer balanced. The average errors for 20^0 angular sectors are listed in Table 6.

The pattern-generating program applies the experimental data to equation (9) with various computer designated illumination functions to find the antenna response at any angle (θ),

$$Y = \sum_{n=0}^{7} (a_n e^{j\alpha_n})(I_{n+1} + jQ_{n+1}) .$$

For uniform weights, $a_n = 1$ and $\alpha = 0$, a broadside beam is formed. This pattern is shown in Figure 35. The pattern conforms to array theory predictions having the first sidelobe 13 dB down from the peak and the second sidelobe about 17 dB down.

Table 6. Average phase and amplitude errors over 200 sectors

RANGE \ ELEMENT	1	2	3	4	5	6	7	8
-90° to 70°	0° 3.5dB	3 0.9	-3 0.1	0 -10	-4 -1.4	5 -1.1	1 -2.0	-2 -2.2
-70° to -50	6 1.3	0 0.5	-6 0.4	0 0.4	-8 0.2	6 0.1	1 -1.3	1 -1.8
-50 to -30	1 0.9	1 1.0	-1 0.5	3 0.5	-8 -0.1	2 -0.3	-1 -1.2	3 -1.7
-30 to -10	6 2.0	3 -0.3	-4 -0.3	0 0.1	-8 -0.6	-3 -0.3	-3 0.0	10 -1.1
-10 to 10	14 0.1	-9 0.0	-1 0.0	-2 0.0	-9 -0.3	0 -0.1	-3 0.1	10 0.0
10 to 30	7 -1.4	1 0.4	-4 0.4	-1 0.4	-9 -0.5	2 0.6	0 -0.3	6 0.3
30 to 50	1 -1.8	4 -0.2	-1 0.3	0 1.0	-10 -0.6	4 0.6	0 0.1	3 0.0
50 to 70	2 -0.9	3 -0.2	-2 -0.3	0 0.3	-9 -1.0	4 0.6	1 0.4	2 0.5
70 to 90	2 -1.3	1 -0.7	-4 -1.1	2 -0.5	-6 -1.3	6 0.8	2 0.7	-2 1.3

Beams can be formed in different directions by adjusting the complex weight a_n. If $a_n = 1$ and the phase of a_n is made equal to $-nkd\sin\theta_0$ the pattern will be maximum in the θ_0 direction. Patterns which demonstrate this scanning feature are shown in Figures 36 through 38 for $\theta_0 = 30^0$, 48^0, and 60^0 respectively. The pattern shape for each of these patterns is similar to that obtained for the broadside beam except that as the beam is scanned there is a loss of gain and a slight increase in sidelobes due to element pattern effects. Figure 39 shows the sum of the magnitude of the elements at each angular position. This envelope is in effect the array element pattern, which is compared to the ideal cosine element pattern. The beamwidth of the element is reduced in the array environment from 112^0 as calculated previously.

Departure of the pattern shown in Figures 35-38 from the ideal are a result of component errors which result in a loss of gain, error in pointing angle and an increase in sidelobe level. For small amplitude and phase errors the effect on gain and pointing is very difficult to measure and quantify; whereas, the error effect on sidelobes is usually dramatic, especially if the sidelobes are designed to be low initially. Consequently, in order to assess the errors, low sidelobe illumination functions such as those described in Section II will be applied to the data to accentuate the error producing effects.

The sidelobes at any point in space, v, can be described statistically [17] to be

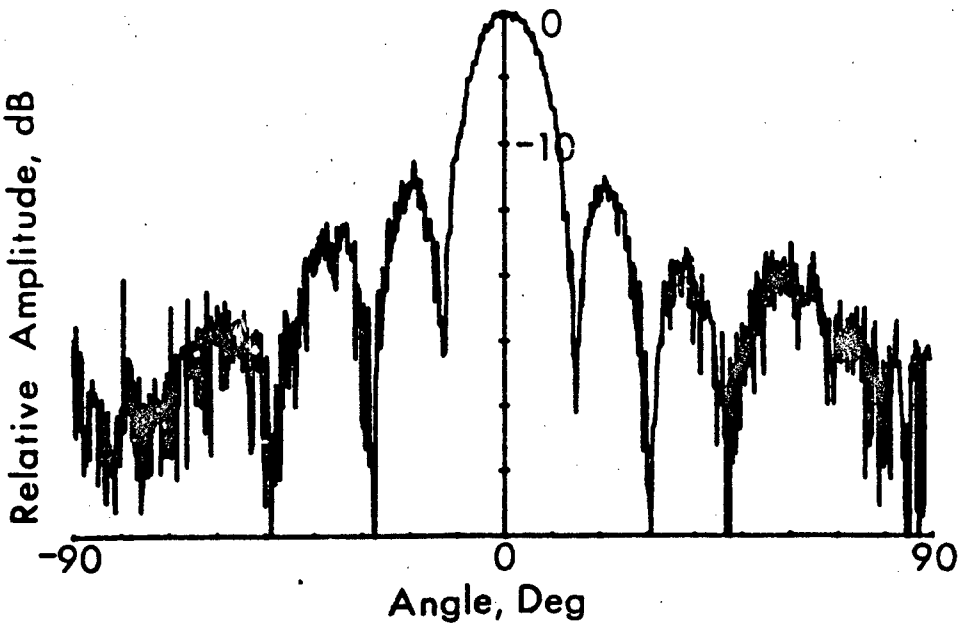

Figure 35. Broadside beam

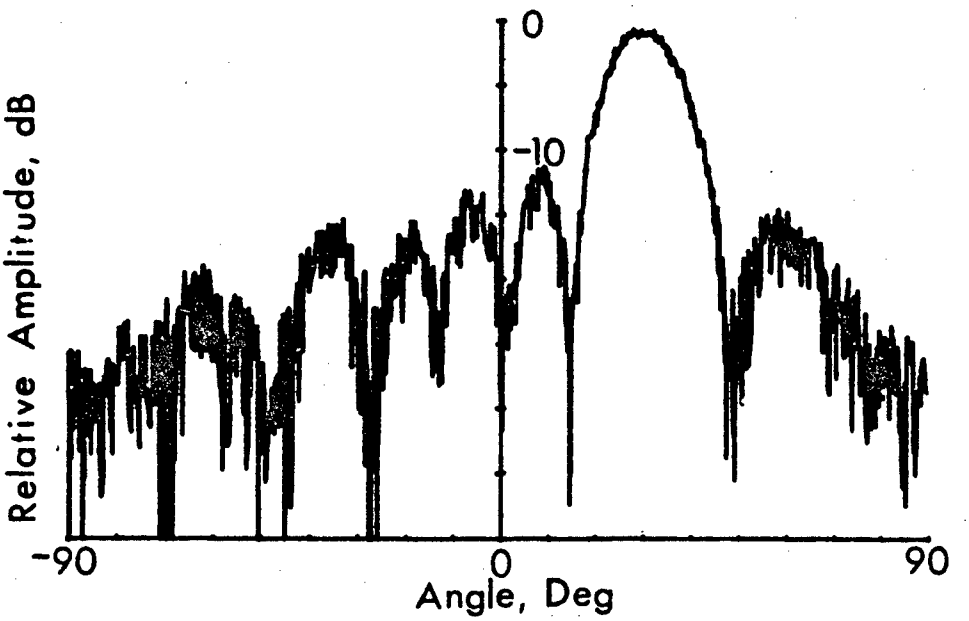

Figure 36. Beam scanned to 30^0 ($\alpha = 90^0$)

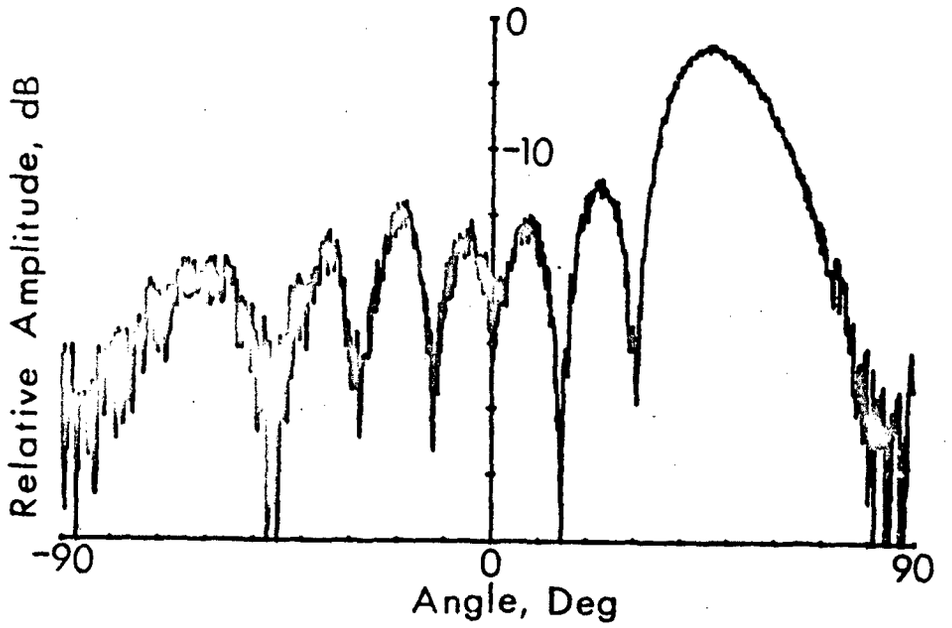

Figure 37. Beam scanned to 48° ($\alpha = 135°$)

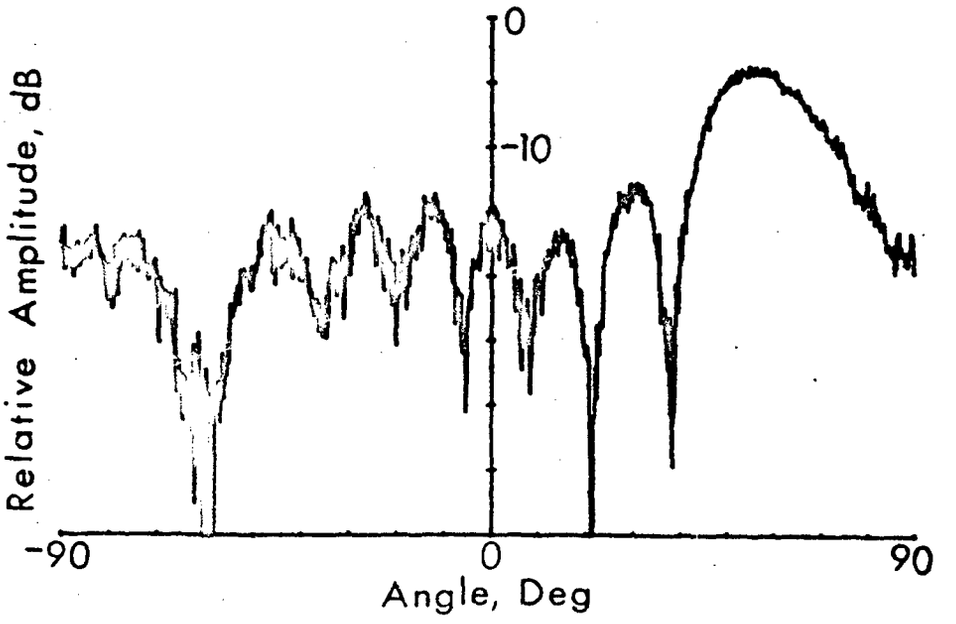

Figure 38. Beam scanned to 60° ($\alpha = 157.5°$)

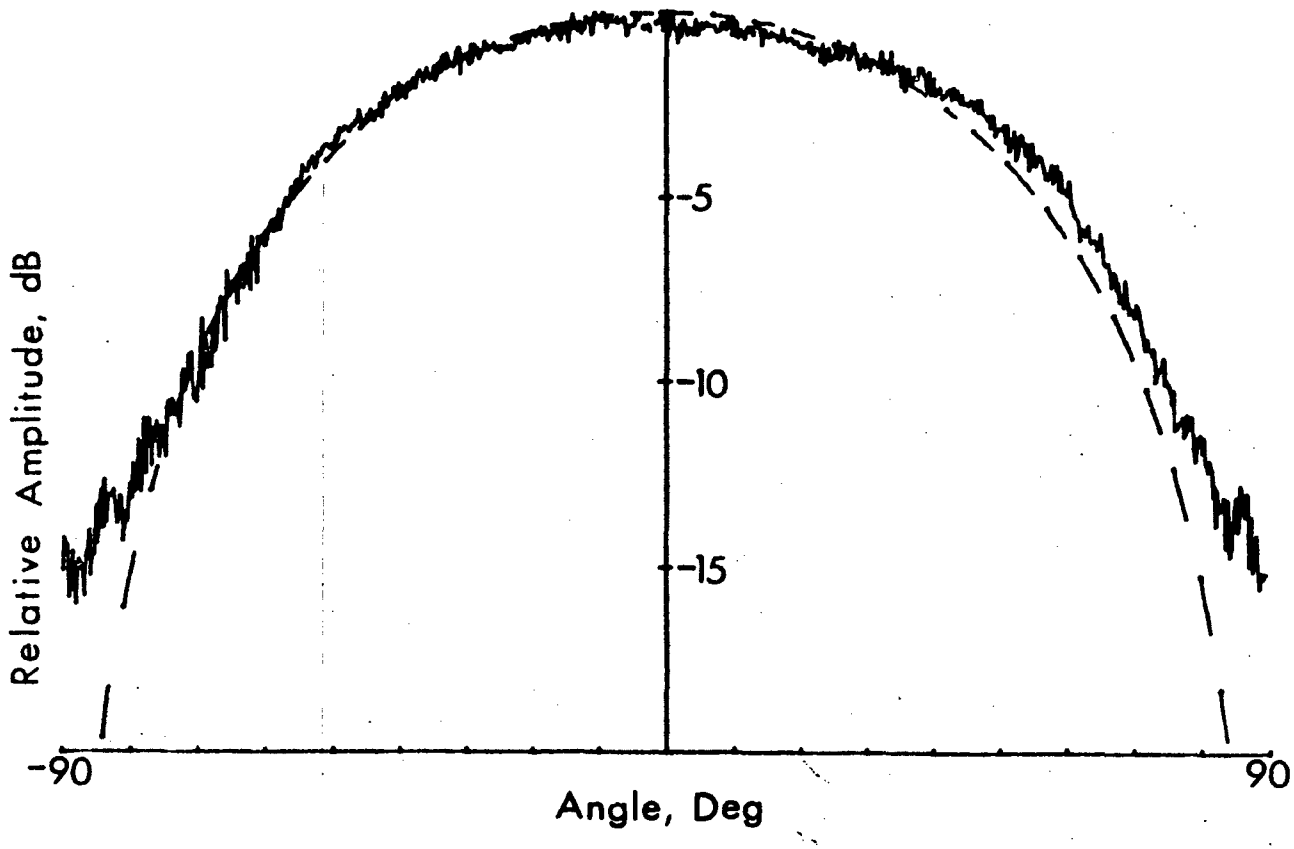

Figure 39. Ideal cosine (dashed) and actual (solid) element pattern

$$p[S(v)] = \frac{S}{\sigma_s} I_o\left(\frac{SS_m}{\sigma_s}\right) \exp\left(-\frac{S^2+S_m^2}{2\sigma_s^2}\right)$$

where $I_o(x)$ is the modified Bessel function, S_m is the design or error free sidelobe level, and σ_s^2 is the variance of the sidelobe level due strictly to the phase and amplitude errors in the array. For small errors

$$\sigma_s^2(v) = \frac{\varepsilon^2(v,t)}{2\eta T} \tag{16}$$

where η is the illumination function efficiency, T is the number of independent elements and $\varepsilon^2(v,t)$ is the sum of the variance of the amplitude and phase errors present in the array; the error is given by

$$\varepsilon^2 = \sigma_A^2 + \sigma_\phi^2$$

where σ_A^2 and σ_ϕ^2 represent the amplitude and phase error variances, respectively; and the arguments of the error terms have been dropped for simplicity.

A threshold sidelobe, S_t, can be established such that

$$p(S_t) = \int_{-\infty}^{S_t} p[S(v)]dS.$$

$P(S_t)$ is the cumulative probability that a sidelobe in direction v will be less than or equal to S_t. A plot of the ratio of S_t^2/S_m^2 as a function of S_m^2/σ_s^2 for several threshold probabilities $S \leq S_t$ is shown in Figure 40. These curves can be used to determine the sidelobe error level, σ_s^2, from which the phase and amplitude errors can obtained.

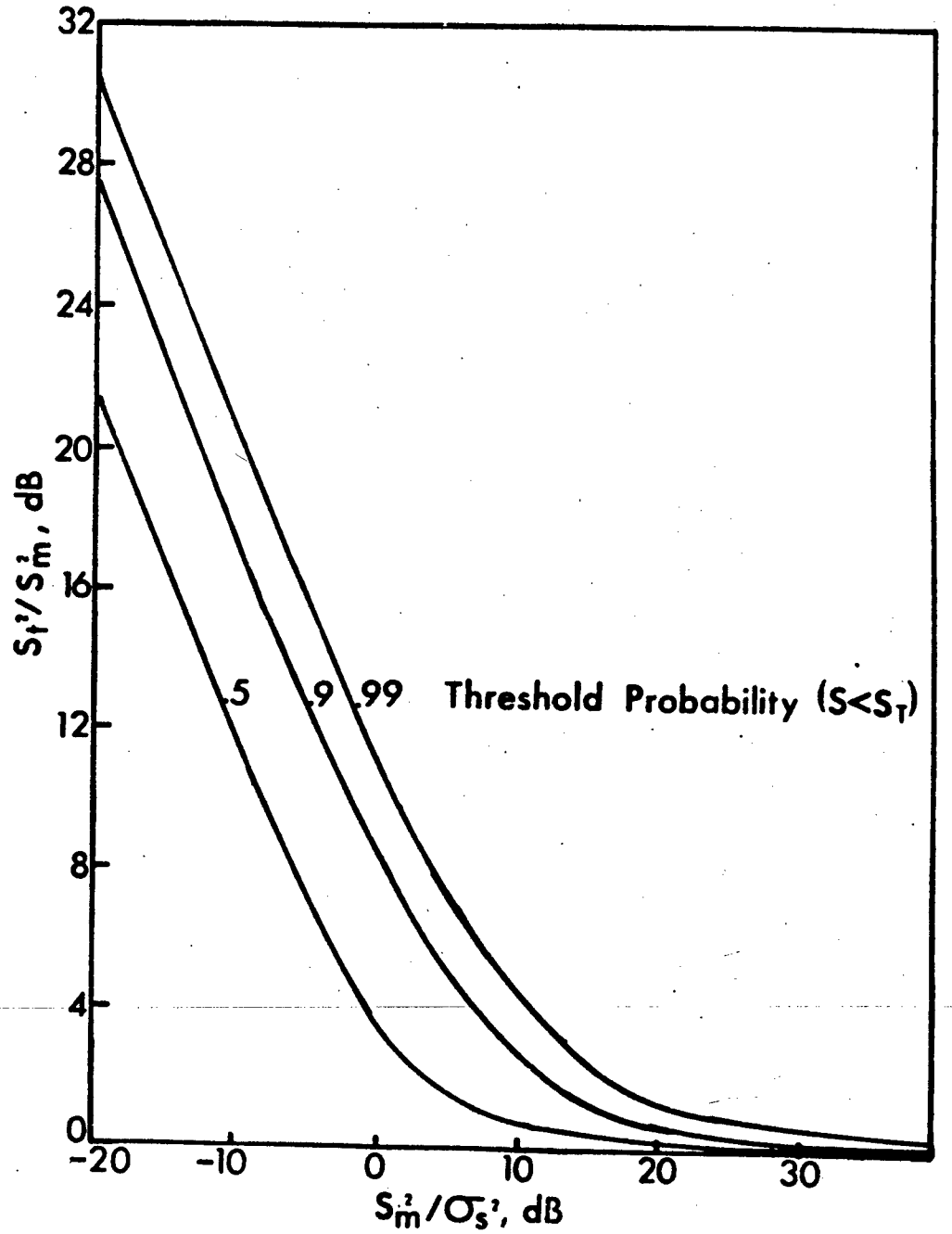

Figure 40. Threshold level relative to design level as a function of scattered energy level

Figure 41 presents the pattern results when a 25 and 30 dB Chebyshev illumination function is applied to the element data. The resulting peak sidelobes are 21 and 23 dB, respectively. Further attempts to reduce the sidelobes by lowering the design level proved fruitless because the error sidelobes far outweigh the design levels beyond 30 dB. The error levels based on these two patterns are calculated below. For the 25 dB case, S_m = -25 dB and S_t = -21 dB at the 99% threshold. Therefore,

$$S_t^2/S_m^2 = -21\,\text{dB} \quad (-25\,\text{dB}\ )$$

$$= 4\ \text{dB}.$$

Using the 0.99 curve of Figure 40 yields $S_m^2/\sigma_s^2 = 10.8$ dB, or

$$\sigma_s^2 = S_m^2 - 10.8\ \text{dB} \tag{17}$$

$$= -25 - 10.8 = -35.8.$$

Relating this value of σ_s^2 to the elemental error through (16) yields

$$\varepsilon^2 = 2\eta T\sigma_s^2$$

$$= 2(.9)8\cdot 10^{-(35.8/10)} \tag{18}$$

$$= 3.79\times 10^{-3}\ \text{rad}^2$$

$$\varepsilon = 3.5^0.$$

Applying the same sequence of calculations to Figure 41b, where S_t is 23 dB and S_m = 30 dB yields

$$S_m^2/\sigma_s^2 = 7\ \text{dB};$$

therefore,

$$\sigma_s^2 = -30 - 5.1 = -35.1\ \text{dB}$$

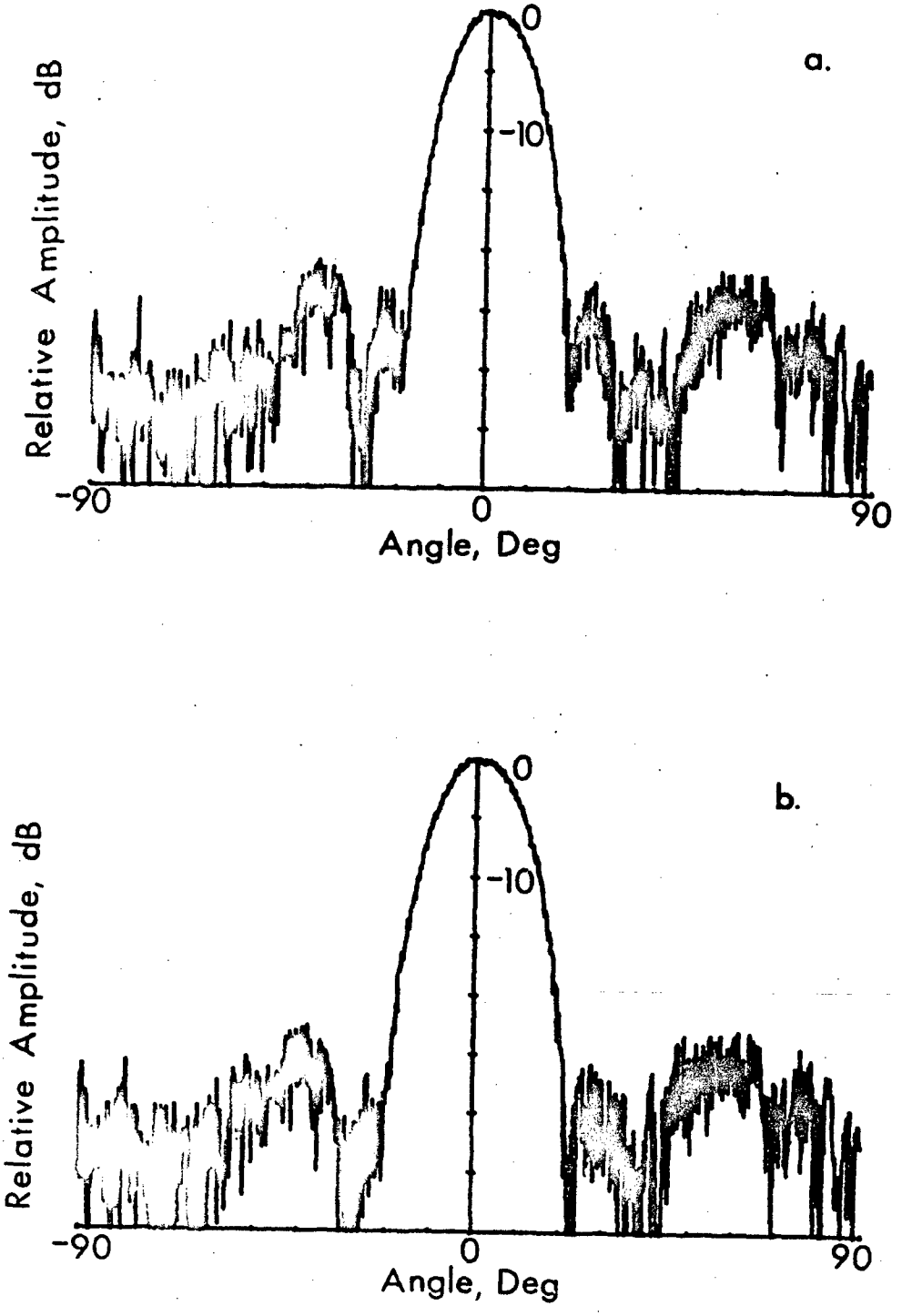

Figure 41. Broadside beam with (a) 25 and (b) 30dB tapers

and the error for the 30 dB pattern ($\eta = 0.85$) is

$$\varepsilon^2 = 2(0.85)8*10^{-(35.1/10)}$$

$$= 4.2*10^{-3}$$

$$\varepsilon = 3.7^{o}.$$

These results are very consistent and indicate that the total component errors in the array are very near 3.6^{o} at this antenna position. The errors varied as a function of antenna position. This was due to a combination of mutual coupling and multipath. The errors corresponding to other angular positions can be verified with respect to Table 6 by again comparing Figure 6 to Figure 41b at positions other than the peak sidelobes.

In order to differentiate between the mutual coupling errors and the other errors, Figure 41 can be compared to Figure 18, which is the pattern derived from only the mutual coupling data. Based on these patterns the rms error due to mutual coupling is about 1.1^{o}. Since these errors are independent of the insertion phase and I and Q sampling variations, the errors due to the insertion and sampling variations can be computed to be

$$\varepsilon_1 = \sqrt{\varepsilon^2 - \varepsilon_c^2}$$

$$= \sqrt{3.6^2 - 1.1^2} \qquad (19)$$

$$= 3.4^{o}.$$

It was described in Section III that the rapid amplitude variations in the sidelobes are caused by a different error set being applied to the array as the received waveform is sampled at different

points. In order to differentiate this I and Q sampling error from the time invariant insertion phase errors, the design level, S_m, is taken to be the average of the fluctuations over a relatively constant portion of the pattern. The angular region between 45 and 65° in Figure 41a and b was selected for the calculations. Following the same procedure as performed in (16) through (18) results in a measured rms I and Q sampling error of 1.7°. Subtracting this error variance from ϵ_1^2 as found in (19) results in an rms insertion phase error of 2.9°. This compares to an error of 3.3° measured on the actual components (see Table 4). Based on the data from Tables 4 and 5, the expected rms error due to I and Q sampling variations for a 10 kHz baseband frequency is 2.0° rms which is very close to the 1.7° computed from the measured data.

Figure 42 which shows the mainbeam scanned in 5° increments, demonstrates the flexibility of DBF processing. The processor is capable of forming beams at all of these positions or any intermediate position in parallel, depending not on parallel microwave hardware but rather on the extent of digital computational hardware.

As described in Section II, a difference pattern can be used when high accuracy is desired. Such a pattern can be produced from the measured element data by weighting the data appropriately. Figure 43 depicts the pattern results when a 30 dB difference pattern illumination function is used. This pattern exhibits an excellent null -35 dB below the peak. The sidelobes are comparable to those obtained when a 30 dB Chebyshev illumination function was used.

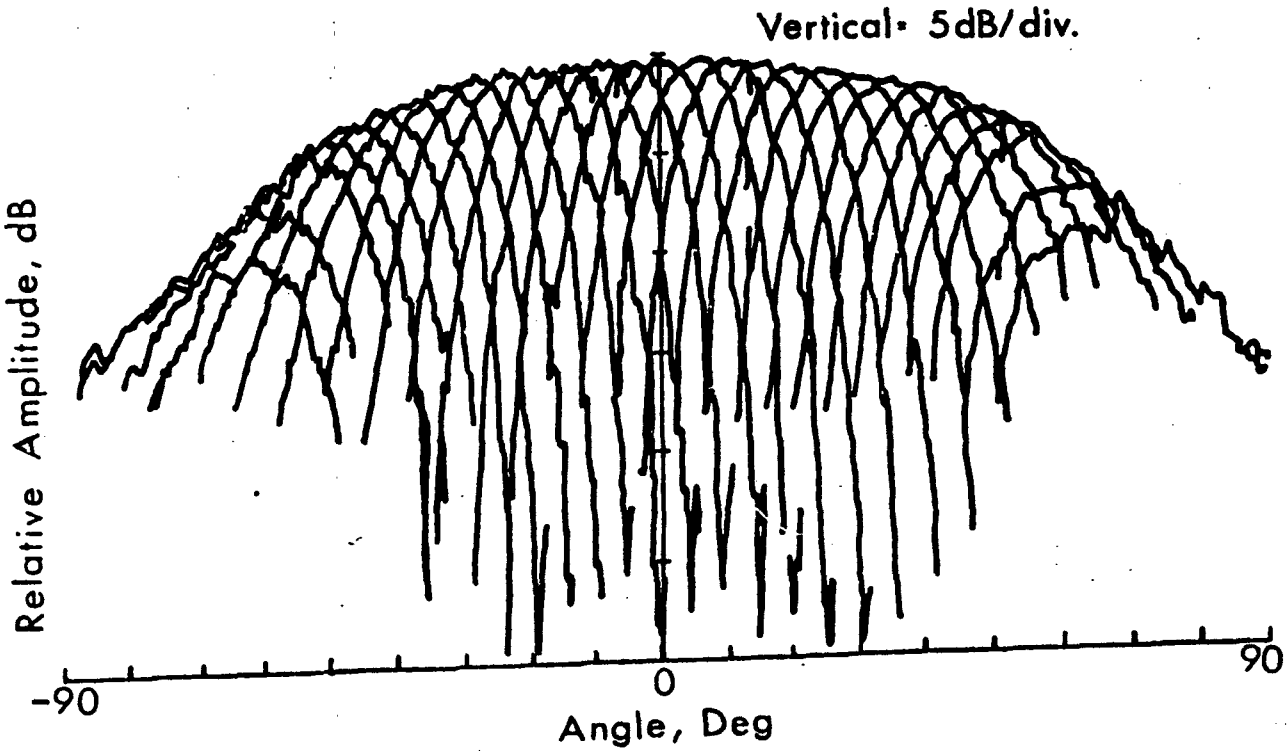

Figure 42. Multiple mainbeams

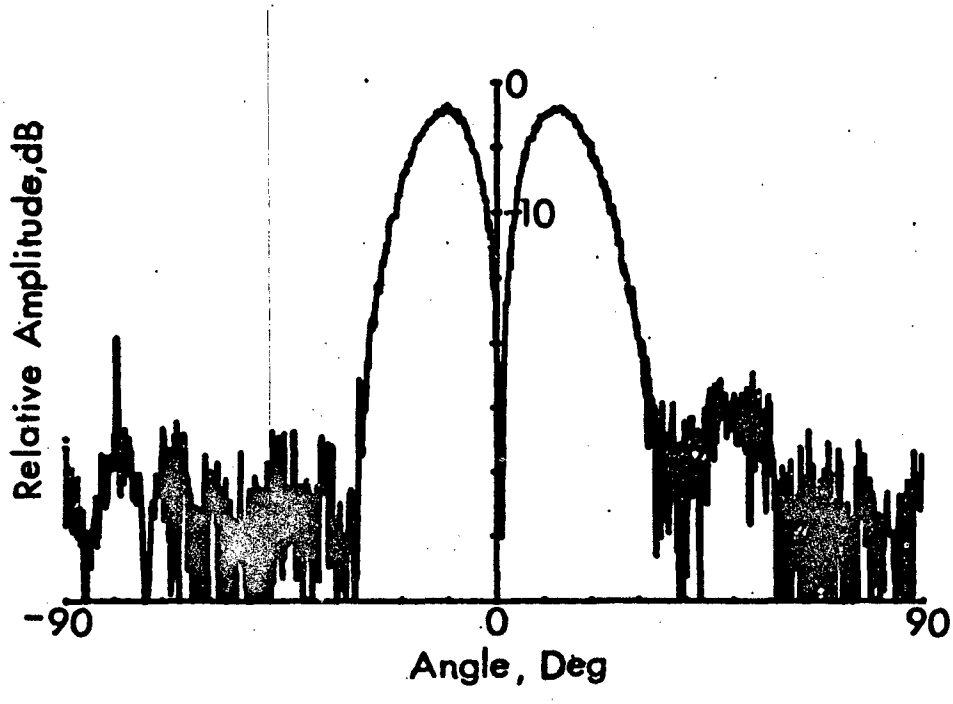

Figure 43. Difference pattern with reduced sidelobes

Table 7 summarizes the rms phase errors in the array system. The measured element to element and I to Q errors are those determined from the direct measurement of the subassemblies (Section III). The measured reflection and coupling errors were determined by combining the terms of the coupling coefficient matrix as outlined in equations 10 through 12. The calculated errors are those determined by applying the statistical error sidelobe analysis of [17] to the measured antenna patterns.

Table 7. Rms phase error summary

Error Source	Measured error, deg	Calculated error, deg
a. Refection and Coupling Coupling	2.6	1.1
b. Element to element down conversion	3.3	2.9
c. I to Q down conversion	1.3	1.7
d. I to Q due to filters	1.5	

The correlation between the measured and calculated errors indicates that the error sources and their effects were fairly well identified although not precisely quantified. The differences were due to measurement accuracy, which was on the order of $\mp 1^{o}$, and the fact that the statistical sidelobe analysis is not as accurate for small arrays as it is for larger arrays. Eight elements did not provide a large enough sample space to determine precisely the sidelobe suppression acheivable in the presence of a specified rms phase error. It did

however provide a method to distinguish the effects of the different phase errors on the antenna patterns.

Each subassembly of the DBF prototype array was designed and built to closely match the phase and amplitude of each receiver in order to characterize the effects of the various errors on the antenna patterns. In an actual system the receivers may not be as closely matched because of cost and reproducibility considerations. A DBF antenna would most likely use a pilot signal scheme to balance both phase and amplitude in each channel. With this technique an equal phase and amplitude pilot signal would be injected into the antenna at RF, and measurements made after A/D conversion would be used for any errors. The I to Q errors in each element could be identified using a technique similar to that described in [18] and the insertion phase and gain errors could then be corrected by multiplying the digitized receive signal by the correction terms.

The errors caused by reflection and coupling could be reduced in one of two ways. First the receiving elements could be designed to minimize the effects of reflection and coupling, this is difficult to accomplish over most scan volumes. Another technique would involve either measuring a central element, in a large array, or each element in a small array before final assembly of the system to determine the reflection and coupling errors. The error data could then be stored in the digital processor and the digitized received signals would again the multiplied by a correction factor this time to reduce the reflection and coupling effects.

V. SUMMARY

An antenna system concept has been described which can provide multiple simultaneous receive beams, with an increased flexibility over the multi-beam systems which generally have spatially fixed multiple beams with fixed beam pattern characteristics. With appropriate signal processing software, a digital beamforming (DBF) system is capable of a combination of automatic and operator designated control over such pattern parameters as beamwidth, null positions, and sidelobe levels, within the limits imposed by the phase and amplitude errors of the system.

An eight element prototype array was designed, built, and tested to experimentally validate the digital beamforming concept and to help identify problem areas. The relative phase and amplitude of the prototype array subassembly were measured and their effects on the antenna patterns were quantified. Errors similar to those in a conventional array were noted along with those which were DBF unique. Pattern data was then gathered and many different pattern types were generated from a single data set. The relationship between design and measured sidelobe levels was used to determine the array errors. These errors were compared with the subassembly measurements to experimentally verify the error producing effects.

LIST OF REFERENCES

1. P. Barton, "Digital Beam Forming for Radar IEE Proc.," Vol 127, Pt. F, No. 4, pp 266-277, August 1980.

2. W. Sander, "Experimental Phased-Array Radar ELRA: Antenna System IEE Proc.," Vol 127, Pt. F, No. 4, pp 285-289, August 1980.

3. D. E. N. Davies, "A Fast Electronically Scanned Radar Receiving System," Br. Inst, Radio Eng, J., Vol 21, pp. 305-318, 1961.

4. W. F. Gabriel, "Adaptive Arrays - An Introduction," Proc, IEEE, Vol 64, pp 239-272, February 1976.

5. R. A. Monzingo and T. W. Miller, Introduction to Adaptive Arrays, John Wiley and Sons, New York 1980.

6. S. M. Kay and S. L. Marple, Jr., "Spectrum Analysis - A Modern Perspective," Proc. IEEE, Vol 69, pp 1379-1419, November 1981.

7. J. E. Evans, J. R. Johnson, and D. F. Sun, "Applications of Advanced Signal Processing Techniques to Angle of Arrival Estimation in ATC Navigation and Surveillance Systems," MIT, Lincoln Laboratory, Lexington, Mass., Technical Report No. 582, June 1982.

8. S. A. Schelkunoff, "A Mathematical Theory of Linear Arrays," Bell System Technical Journal, Vol 22, pp 80-107, January 1943.

9. L. B. Brown and G. A. Scharp, "Chebyshev Antenna Distribution, Beamwidth, and Gain Tables," Nav. Ord. Report 4629, Corona, California, February 1958.

10. D. K. Barton and H. R. Ward, Handbook of Radar Measurements," Prentice-Hall, Englewood Cliffs, New Jersey, 1969, p 247.

11. R. S. Elliott, Antenna Theory and Design, Prentice-Hall, Inc, Englewood Cliffs, New Jersey, 1981.

12. J. L. Butler, "Digital, Matrix, and Intermediate Frequency Scanning," of Microwave Scanning Antennas, Vol III, edited by R. C. Hansen, Academic Press, New York, 1966, Ch. 3.

13. W. Rotman and R. F. Turner, "Wide Angle Lens for Line Source Applications," IEEE Trans., Vol AP-11, pp 623-632, November 1963.

14. R. S. Packard, and R. V. Lowman, "Transmission Lines and Waveguide," of Antenna Engineering Handbook, edited by H. Jasik, McGraw Hill, New York, 1961, pp 30-38.

15. A. A. Oliner and R. G. Malech, "Mutual Coupling in Infinite Scanning Arrays," of Microwave Scanning Antennas, Vol II, edited by R. C. Hansen, Academic Press, New York, 1966, Ch. 3.

16. R. J. Polge, L. Callas, B. K. Bhagavan, and E. R. McKee, "Analog-to-Digital Converter Evaluation by Digital Computer Analysis of Recorded Output," UAH Research Report No. 149, February 1974.

17. J. L. Allen, "Phased Array Radar Studies," MIT, Linclon Laboratory, Lexington, Mass., 1960-61.

18. F. E. Churchill, G. W. Ogar, and B. J. Thompson, "The Correction of I and Q Errors in a Coherent Processor," IEEE Trans., Vol AES-17, No. 1, pp 131-137.

DISTRIBUTION

Defense Documentation Center 12
Cameron Station
Alexander, VA 22314

Air Force Avionic Laboratory 1
ATTN: AADM, Harold Weber
Wright-Patterson Air Force Base, OH 45433

Commandant 1
US Army Air Defense Artillery
ATTN: ATSC-CDM-A, Toney LePreste
Fort Bliss, TX 79916

Defense Advanced Research Projects Agency
ATTN: Tactical Technology Office
LTC Jurgen Gobien 1
Verne L. Lynn 1
Theo Kooij 1
1400 Wilson Blvd
Arlington, VA 22209

Commander
US Army Materiel Development and Readiness Command
ATTN: DRCLDC, Jim Bender 1
5001 Eisenhower Avenue
Alexandria, VA 22333

Rome Air Development Center
ATTN: OC, Frank Rhem 1
OCDE, John Clancey 1
OCDE, Gary Plotz 1
Griffiss Air Force Base, NY 13441

Commander, Harry Diamond Labs 1
ATTN: DELHD-RT-RC, Jim Shreve
2800 Powder Mill Road
Adelphi, MD 20783

Director, Naval Research Lab
ATTN: I.D. Olin, Code 5301 1
P. Shelton, Code 5304 1
B. Waters, Code 5330.1W 1
Washington, DC 20375

Naval Air Development Center 1
ATTN: Dr. John Smith, Code 3022
Warminster, PA 18974

Naval Ocean Systems Center ATTN: Dr. Wehner, Code 732 San Diego, CA 92152	1
Commander Naval Sea Systems Command ATTN: SEA-61 DE, R. T. Hill Washington, DC 20362	1
Lincoln Laboratories ATTN: I. Stiglitz P. O. Box 73 Lexington, MA 02173	1
Naval Electronics Lab Center ATTN: Library San Diego, CA 95152	1
US Naval Ordnance Laboratory ATTN: Technical Library White Oak, Silver Spring, MD 20910	1
Commandant, Marine Corps ATTN: Code A04C HQ Washington, DC 20380	1
Rome Air Development Center ATTN: EEA, Bob Mallioux EEA, Hans Steyskal Hanscom Air Force Base, MA 01731	1 1
US Army Aviation Research and Development Command ATTN: DRBAV-NC, Dr. Gene Marner 4300 Goodfellow Blvd St. Louis, MO 63120	1
Headquarters US Army CS&TA Laboratory ATTN: DELCS-R, W. Fishbein Ft. Monmouth, NJ 07703	1
DRSMI-R Dr. McCorkle	1
-R Dr. Rhoades	1
-RR Dr. Hartman	1
-RR Dr. Duthie	1
-RAR Mr. Tippit	1
-RGS Mr. Dihm	1
-RE Mr. Lindberg	1
-RE Mr. Pittman	1
-ROA Mr. Peterson	1
-RER Mr. Rose	30
-RPT Record Copy	1
-RPR	1
BMDATC-RR Mr. King	1
-P Mr. McKay	1